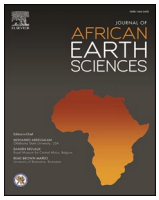
Journal of African Earth Sciences 229 (2025) 105674



Contents lists available at ScienceDirect

Journal of African Earth Sciences

journal homepage: www.elsevier.com/locate/jafrearsci



Neogene sedimentary evolution and biostratigraphy of the Kasaba and Aksu-Gebiz basins in the eastern Mediterranean: Insights from paleontology and Sr isotope stratigraphy

Ahmet Can Akıncı [a,*], Nusret Nurlu [a], Ulvi Can Ünlügenç [a], Deniz İbilioğlu [b], Hande Sonsun [a]

[a] Çukurova University, Faculty of Engineering, Geological Engineering Department, Sarıçam, Adana, Turkey
[b] Dumlupınar University, Geological Engineering Department, 43100, Kütahya, Türkiye

ARTICLE INFO

Handling Editor: M Mapeo

Keywords:
Eastern Mediterranean
Kasaba Basin
Aksu-Gebiz Basin
Planktonic foraminifera
Strontium isotope chemostratigraphy
Stratigraphy
Neogene basins

ABSTRACT

The Kaş-Kasaba and Aksu-Gebiz basins are two important Neogene basins in the Eastern Mediterranean, flanking the Gulf of Antalya in southwestern Anatolia. Comprehensive studies involving sedimentology, paleontology, and Sr isotopes have offered valuable insights into the sedimentary characteristics and depositional environments of these basins during the Neogene period. In the west, the Kasaba Basin features an early to middle Miocene carbonate-clastic succession that developed on the Late Cretaceous Beydağları autochthon, overlain by Paleocene-Eocene neritic carbonates. In contrast, the Aksu-Gebiz Basin in the east presents a transgressive sequence of middle Miocene to Pliocene clastics and carbonates, which developed on different basement units, including the Mesozoic metamorphosed carbonates and the Antalya Complex in the west. Biostratigraphic studies in the Kasaba (Kaş) region revealed 9 genera and 23 species of planktonic foraminifera in the Kasaba Formation, and 12 genera and 29 species in the Sinekçi Fm., marking the lower boundary of the *Orbulina suturalis* Lineage Subzone (MMi5a) of the middle Miocene. Similarly, in the Gebiz (Aksu) region, the planktonic foraminifera indicate the lower boundary of the MMi12a *Globigerinoides obliquus extremus-Globorotalia suterae* Interval Subzone of the late Miocene. Benthic foraminifera indicative of shelf environments were identified in both regions. Whole-rock strontium isotope chemostratigraphy revealed ages ranging from 14.3 to 23.7 Ma based on $^{87}Sr/^{86}Sr$ ratios from three key samples. Overall, studies in the Kasaba Basin suggest a lower to middle Miocene age with shallow marine environments, consistent with Serravallian to Langhian periods. In the Aksu-Gebiz Basin, detailed investigations of the Karpuzçay Formation identified a mid-Tortonian age. This age, combined with sedimentological and structural data, provides insights into the basin's tectonic evolution and flexural effects. Planktonic and benthic foraminifera within the sequence reflect inner shelf environments throughout. The strontium isotope analysis of samples from the Aksu-Gebiz Basin revealed significant variations in $^{87}Sr/^{86}Sr$ ratios, with ages ranging from the Tortonian (9.0 Ma) to the Messinian (5.3 Ma). By integrating biostratigraphy and whole-rock Sr isotope stratigraphy, this study refines the Neogene chronological framework of the Kasaba and Aksu-Gebiz Basins, providing new insights into the Eastern Mediterranean's geological history. These findings also improve stratigraphic correlations with adjacent basins, offering a more comprehensive regional context.

1. Introduction

$^{87}Sr/^{86}Sr$ have been widely used to date and correlate carbonate successions, particularly in the last three decades (e.g. Burke et al., 1982; De Paolo and Ingram, 1985; McArthur et al., 1994; Howarth and McArthur, 1997; McArthur et al., 2001, 2012; Dill et al., 2003; Dill and Henjes-Kunst, 2007; Frijia and Parente, 2008; Brandano and Policicchio, 2012). The $^{87}Sr/^{86}Sr$ ratio in the global ocean has varied through the geological time (McArthur et al., 1994, 2012) and the world's oceans are homogeneous with respect to $^{87}Sr/^{86}Sr$ ratio, and this is assumed for any geologic time (McArthur et al., 2012). Consequently, the Sr isotope composition is widely used to support paleontology to date marine minerals, correlate marine sedimentary sequences around the world (Faure and Mensing, 2005). Application of Sr isotope stratigraphy

* Corresponding author.
E-mail address: acakinci@cu.edu.tr (A.C. Akıncı).

https://doi.org/10.1016/j.jafrearsci.2025.105674
Received 19 September 2024; Received in revised form 21 April 2025; Accepted 24 April 2025
Available online 2 May 2025
1464-343X/© 2025 Elsevier Ltd. All rights are reserved, including those for text and data mining, AI training, and similar technologies.

requires measurement of the Sr isotope ratio ($^{87}Sr/^{86}Sr$) of minerals that directly precipitated from seawater and have not undergone diagenetic alteration of their original $^{87}Sr/^{86}Sr$ value. Some geologic periods such as the Miocene, are especially useful for the application of Sr isotopic stratigraphy as they display a narrow error interval on the reference curve (McArthur et al., 2012), allowing quite accurate age constraints. The $^{87}Sr/^{86}Sr$ in sea water is mainly controlled by two different factors: continental weathering and ocean floor hydrothermal exchange and volcanism (Faure, 1986; Palmer and Edmond, 1989; Taylor and Lasaga, 1999). The continental weathering tends to increase the $^{87}Sr/^{86}Sr$ ratio, while volcanism transport considerable amounts of light ^{86}Sr, lowering the Sr isotope ratio.

The eastern Mediterranean region (Fig. 1) is part of the Afro-Eurasian collision zone (Fig. 2) (e.g., Ben-Avraham, 1978; Khain, 1984; Garfunkel, 1998), containing oceanic rift systems and terrane belts (Stampfli et al., 2013). The eastern Mediterranean Sea and some of the landmass in the region (Fig. 1) is the remnant of the Neotethyan oceanic tract that once separated the Eurasian and African plates (Robertson and Kopf, 1998). Convergence occurred by subduction of the intervening oceanic lithosphere and by squeezing of microplates caught in between. The present-day tectonic framework represents the last phase of this convergence and the displacements of the smaller microplates (Robertson and Dixon, 1984; Dewey et al., 1986; Robertson et al., 1998a, 1998b; Glover and Robertson, 1998; Akıncı et al., 2003; Reilinger et al., 2006; Güneş et al., 2018). Today, the last remnants of the Neotethys Ocean are subducting beneath the Eurasian Plate across the western sector of the Aegean–Anatolian Microplate, but subduction stalled across the Cyprus Arc, caused by incipient collision of the Eratosthenes micro-continental block with the Island of Cyprus. Miocene is a key interval in the geodynamic evolution of the Mediterranean basin as it has widely shaped the region's recent geological framework. Studies on sedimentary successions and diagenetic processes in the Arabian Plate margin offer valuable insights into the geological evolution of Neogene basins in southwestern Anatolia. Dill et al. (2003) identified transgressive-regressive cycles and sequence stratigraphic bounding surfaces in the Dukhan Anticline, reflecting depositional shifts that parallel those observed in the study area. The application of Sr isotope stratigraphy by Dill and Henjes-Kunst (2007) in the Miocene Dam Formation of Qatar demonstrates its effectiveness in refining stratigraphic correlations, reinforcing its utility in constraining the Neogene sequences of the Kasaba and Aksu-Gebiz Basins. Boulton et al. (2007) used strontium isotope stratigraphy and micropaleontology to refine the stratigraphy of the Hatay Graben, highlighting Sr isotopes' role in constraining depositional ages and tectonic influences, which is relevant to this study. Furthermore, Dill et al. (2009) examined diagenetic and epigenetic alterations in organic-rich successions of northwestern Jordan, highlighting fluid-rock interactions that influenced lithological evolution. These studies provide a valuable comparative framework for assessing the stratigraphic architecture, diagenetic overprints, and geochemical characteristics of the study area.

The Miocene Kasaba Basin, located in southwestern Turkey, is a peripheral foreland basin that resulted from the thrusting and emplacement of the Lycian Nappes, a complex stack of thrust sheets, onto a previously stable carbonate platform (Hayward, 1984; Ersoy, Ş., 1990; Aksoy and Aksarı, 2008). The Lycian Nappes contain not only ophiolitic material but also carbonate and clastic units, contributing to the formation of the basin. Instability occurred during the latest Cretaceous and Eocene, as noted by previous studies (e.g., Collins and Robertson, 1998). The resulting basin-fill is the product of the complex interaction of tectonic and sedimentary processes and records the timing and magnitude of tectonic events in the thrust belt (Woodcock and Robertson, 1977; Robertson, 2000; Şenel et al., 1991; 2004; Aksoy and

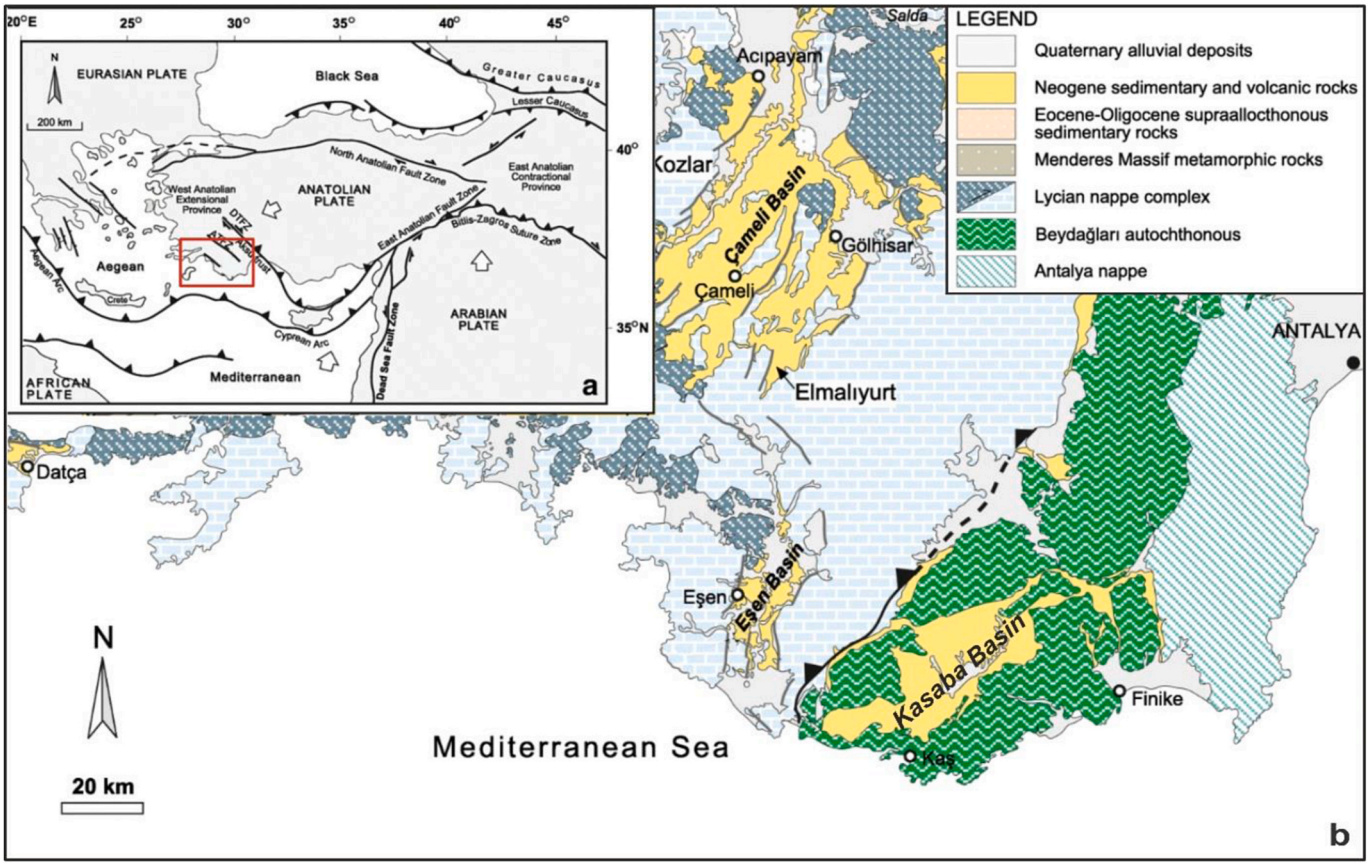


Fig. 1. a) Outline tectonic map showing the major tectonic elements of the SW Anatolia region (Bozkurt, 2003; Alçiçek et al., 2017, 2019; Kaymakçı et al., 2018); b) Overview of the main Cenozoic basins of SW Anatolia region (based on Konak, 2002; Konak and Şenel, 2002; Şenel, 2002; Alçiçek et al., 2019).

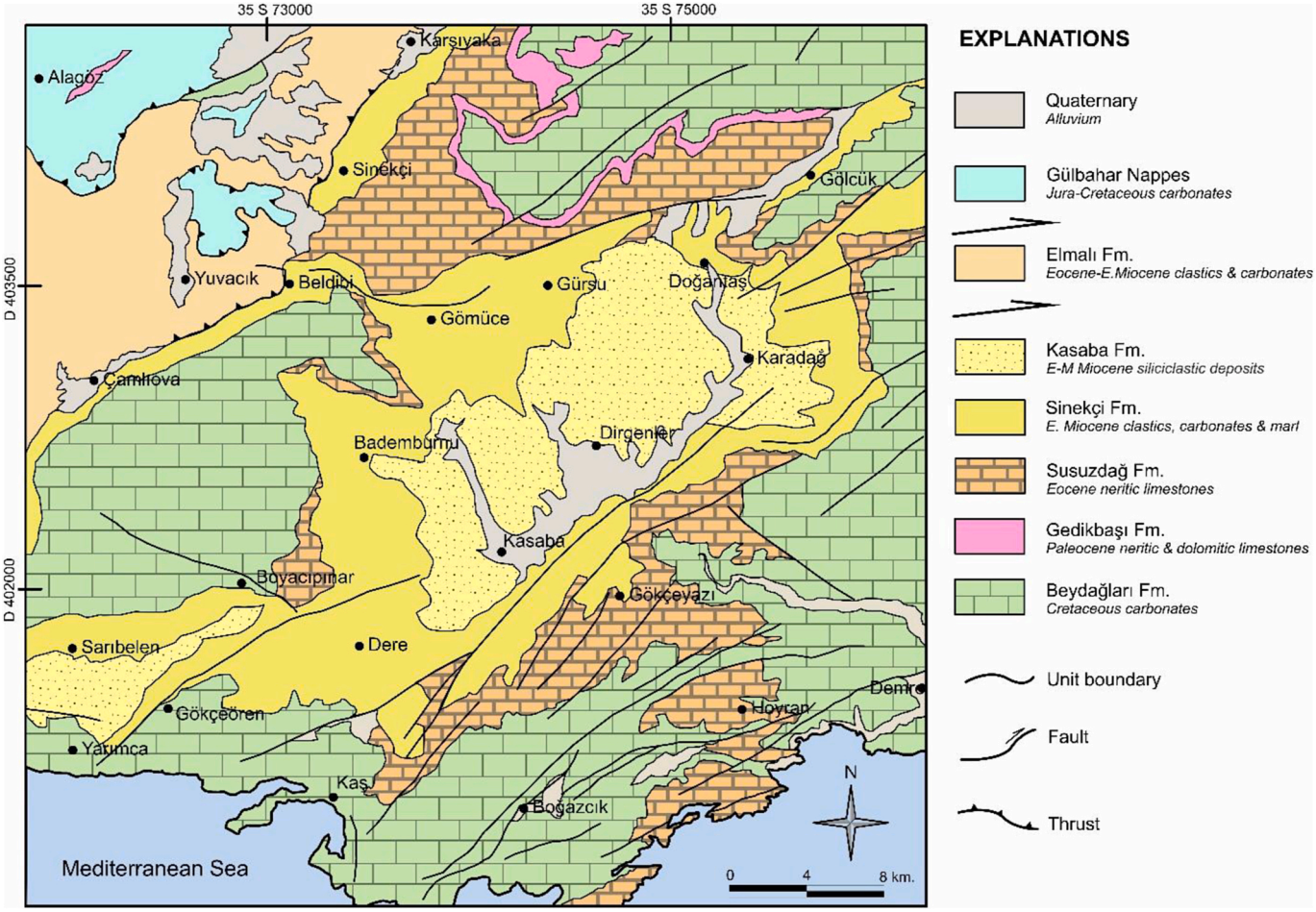


Fig. 2. Geological map of the Kasaba Basin and surrounding region (modified after İslamoğlu and Taner, 2002a,b; İslamoğlu, 2004; Üner et al., 2018).

Aksarı, 2008; Robertson et al., 2024). Clastic and carbonate deposits of the Kasaba basin are well exposed in the Kasaba syncline, beneath the present-day thrust front of the Lycian Nappes. A more detailed stratigraphic construction of the units outcropping in the basin, combined with updated and more precise age data, will provide a clearer understanding of the basin's evolution and the tectonic and sedimentary processes that have shaped it.

Bordering the eastern flank of the Antalya Gulf, the Aksu/Manavgat Basin, located within the Isparta Angle, has developed unconformably over the Antalya, Beyşehir-Hoyran-Hadım Nappes since the late Cenozoic (Dumont and Kerey, 1975; Woodcock and Robertson; 1977; Akay et al., 1985a, 1985b; Monod et al., 2006; Çiner et al., 2008; Poisson et al., 2011; Hall et al., 2014). This basin is one of the two subbasins of the Antalya Basin (the other being Köprüçay), and it features two major structural elements: The Kırkkavak Fault, which strikes north-south, and the Aksu Thrust, which verges west to southwest (Üner et al., 2018). The Aksu-Manavgat Basin has undergone four distinct stages of structural evolution (Üner et al., 2015, 2018). The first phase, characterized by NW-SE directed compression due to the emplacement of the Lycian Nappes, lasted until the Langhian. This was followed by a NW-SE extensional stress regime between the Langhian and Messinian, succeeded by a NE-SW compressional stress regime known as the Aksu Phase. The neotectonic period, commencing in the Late Pliocene, is marked by NE-SW extension (Üner et al., 2015; Yılmaz et al., 2024). The complex tectonic history of the Aksu Basin has significantly influenced its sedimentary features, with notable formations including the Eskiköy alluvial fan and the Kapıkaya, Kozan, Karadağ, Kargı, and Bucak fan deltas. While the Eskiköy alluvial fan and Kapıkaya, Kozan, and Bucak fan deltas evolved under a single extensional regime, the Karadağ and Kargı fan deltas were shaped by all the tectonic phases experienced by the Aksu Basin (Şenel, 1997; Poisson et al., 2003; Karabıyıkoğlu et al., 2005; Çiner et al., 2008).

This study aims to elucidate the sedimentary evolution and depositional history of the Kaş-Kasaba and Aksu-Gebiz basins in the Eastern Mediterranean, providing key insights into the Neogene geological development of southwestern Anatolia. To achieve this, an integrated biostratigraphic framework is presented, evaluating the $^{87}Sr/^{86}Sr$ isotopic data of the analyzed sedimentary rocks with their sedimentological and stratigraphic relationships.

2. Geological background

The Miocene Kasaba Basin, situated on the Teke Peninsula in the Western Taurus region of Turkey, extends approximately 25–30 km in a northeast-southwest direction, north of Kaş (Fig. 1). The basin is structurally controlled by NE-SW trending fault systems, particularly along its east-southeast boundary, extending toward Çağman. The surrounding geology comprises allochthonous and autochthonous marine sediments ranging from the Jurassic to the middle Miocene (Collins and Robertson, 1998; İslamoğlu ve Taner, 2002; İslamoğlu, 2004; Aksarı, 2007; Aksoy ve Aksarı, 2008; Darbaş ve Gül, 2017; Robertson et al., 2024). The main tectonostratigraphic units in the region include the Beydağları autochthon, the Yeşilbarak nappe, and the Lycian nappe (Colin, 1962; Şenel et al., 1989, 1994; Flecker et al., 1995; Şenel, 1997; Tunoğlu ve Bilen, 2001; Durutürk, 2018).

The regionally extensive Beydağları autochthon unit has been studied in detail by numerous researchers (Colin, 1962; Poisson, 1977; Önalan, 1979; Erakman et al., 1982; Günay et al., 1982; Yalçınkaya

et al., 1986; Şenel et al., 1989, 1994; Sarı and Özer, 2009). The Miocene succession in the study area unconformably overlies a basement composed of Jurassic to Paleogene carbonates, primarily consisting of platform limestones and dolomitic limestones (Önalan, 1979; Şenel et al., 1989, 1994; Şenel, 1997). The lower Miocene sequence begins with shallow marine carbonates and marls of the Burdigalian Sinekçi Formation (Önalan, 1979; Şenel et al., 1989, 1994), which is subdivided into distinct members representing varying depositional conditions. These units transition into fine-to coarse-grained siliciclastic deposits of the late Burdigalian to Langhian Kasaba Formation, indicating a regressive trend with abundant benthic foraminifera, ostracods, and mollusks (İslamoğlu and Taner, 1999, 2002). In the southwest of the study area, the Kasaba Formation is unconformably overlain by the conglomeratic deposits of the late Langhian Felenkdağ Formation (Şenel et al., 1989, 1991), while in the north-northwest, it is tectonically juxtaposed with the allochthonous units of the Yeşilbarak Nappe.

Partly exposed within the study area (as Elmalı Fm. in the NW part) (Fig. 2), the Yeşilbarak Nappe extends laterally between the Beydağları autochthon and the Lycian nappes (Poisson, 1977; Önalan, 1979; Şenel et al., 1989, 1994, 1997). This nappe predominantly consists of clastic deposits with a turbiditic character and ranges in age from the upper Lutetian to the lower Miocene. The Yeşilbarak Nappe is structurally divided into two units: The Gömbe Group and the Yavuz Formation (Şenel et al., 1989). The Gömbe Group is underlain by the Cenomanian to Santonian (late Cretaceous) Gebeler Formation. Overlying the Gebeler Formation is the transgressive Elmalı Formation, which dates from the late Lutetian to the early Miocene and is exposed around Gömbe and Elmalı, in the western and northwestern parts of the Kasaba Basin (Önalan, 1979; Şenel et al., 1989, 1994). The Uçarsu Formation, which both conformably and unconformably overlies the Elmalı Formation, is exposed to the east and southeast of Mount Akdağ and around Bozgediktepe village. The Uçarsu Formation is characterized by its regressive nature and is dated to the late Burdigalian, based on paleontological evidence (İslamoğlu and Taner, 1999, 2002).

The Lycian nappes, extensively exposed to the north and northwest of the Kasaba Basin, consist of several tectonic units, including the Tavas, Bodrum, Dumanlıdağ, Marmaris ophiolite, Gülbahar, and Domuzdağ nappes (Şenel et al., 1987, 1989, 1994; Konak et al., 1990).

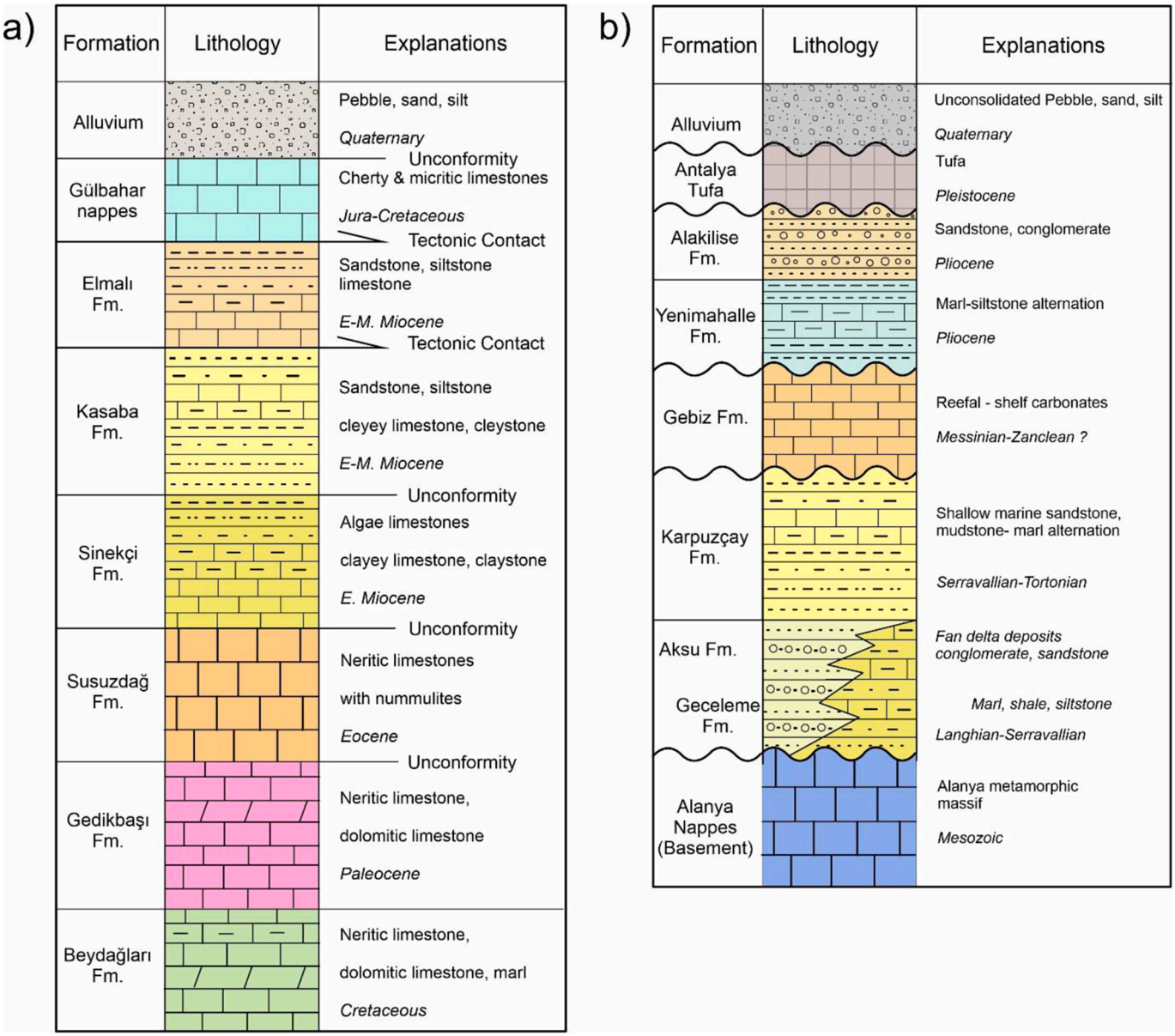


Fig. 3. Stratigraphic columnar sections of the units exposed around the a) Kasaba Basin, b) Aksu-Gebiz Basin.

The Dumanlıdağ nappe, forming the tectonic base of the Lycian nappes, is primarily exposed in and around the Akdağ area. The Gülbahar nappe, characterized by cherty-micritic limestones, tectonically overlies the Elmalı Formation of the Yeşilbarak nappe in the northwesternmost part of the study area (Figs. 2 and 3). These nappes play a crucial role in the geological framework influencing the evolution of Miocene basins in the region. Poisson (1977) previously described these units under different names in his PhD study conducted across the western Taurides, highlighting variations in their classification across studies.

Therefore, the Sinekçi and Kasaba formations, which are Miocene units rich in microfauna, were studied in detail, and four stratigraphic sections were measured in the Kasaba Basin. In this study, the systematic characteristics and depositional environments of these units, based on the identified fauna, were described, and their biostratigraphy was examined according to the levels at which they were found.

The measured sedimentary logs from the Kasaba Basin (Fig. 4), document a transition from carbonate-dominated shallow marine environments to siliciclastic deposition, reflecting a regressive trend from the Burdigalian to Langhian. The Susuzdağ Formation, consists of nummulitic limestones indicative of a warm, shallow neritic environment. The overlying Sinekçi Formation, represented by two logs, comprises fossiliferous limestone successions with abundant foraminifera, gastropods, and bivalves, confirming a continued shallow marine setting with occasional energy fluctuations. Sampling for Sr isotope analysis was conducted from these levels. The presence of bioturbation and minor cross-lamination suggests periodic water agitation and sediment reworking. A significant shift occurs with the deposition of the Kasaba Formation, which overlies the Sinekçi Formation and marks a transition to fine-to coarse-grained siliciclastic deposits. This unit, characterized by sandstones, siltstones, and claystones interbedded with fossil-rich horizons, reflects a progradational regressive system associated with increased terrestrial input and shallowing conditions. The prevalence of benthic foraminifera, ostracods, mollusks, and corals further supports deposition in a high-energy nearshore to coastal setting. The Km-1 sample for Sr isotope analysis was collected from the carbonate levels at the basal sections of this log. The progressive coarsening-upward trend suggests sediment influx from a continental source, likely driven by regional tectonic uplift and sea-level fluctuations. Overall, the stratigraphic succession recorded in the logs captures the paleoenvironmental evolution of the Kasaba Basin, transitioning from a warm, carbonate platform to a siliciclastic-dominated regressive system influenced by tectonics and sediment supply dynamics.

Approximately 130 km east of the eastern flank of the Antalya Gulf lies another significant basin, the Aksu-Gebiz Basin (Fig. 5), which extends in a N-S direction. The Aksu Basin is located within the Isparta Angle, which is one of the most important morphotectonic structures in Southwest Anatolia. This reverse V-shaped structure, first defined by Blumenthal (1951), is situated north of Antalya Bay, at the intersection of the Cyprus and Aegean arcs in the Eastern Mediterranean. The Isparta Angle is structurally closely related to the NW-trending Akşehir Fault Zone in the east, being part of the Western Anatolian Extensional Province (Koçyiğit and Özacar, 2003; Özsayın and Dirik, 2007, 2011; Özsayın et al., 2013; Üner et al., 2018). While some studies have proposed the existence of the Fethiye-Burdur Fault Zone in the northeast (Barka et al., 1997), recent research challenges its existence, suggesting that the region is dominated by extensional deformation rather than

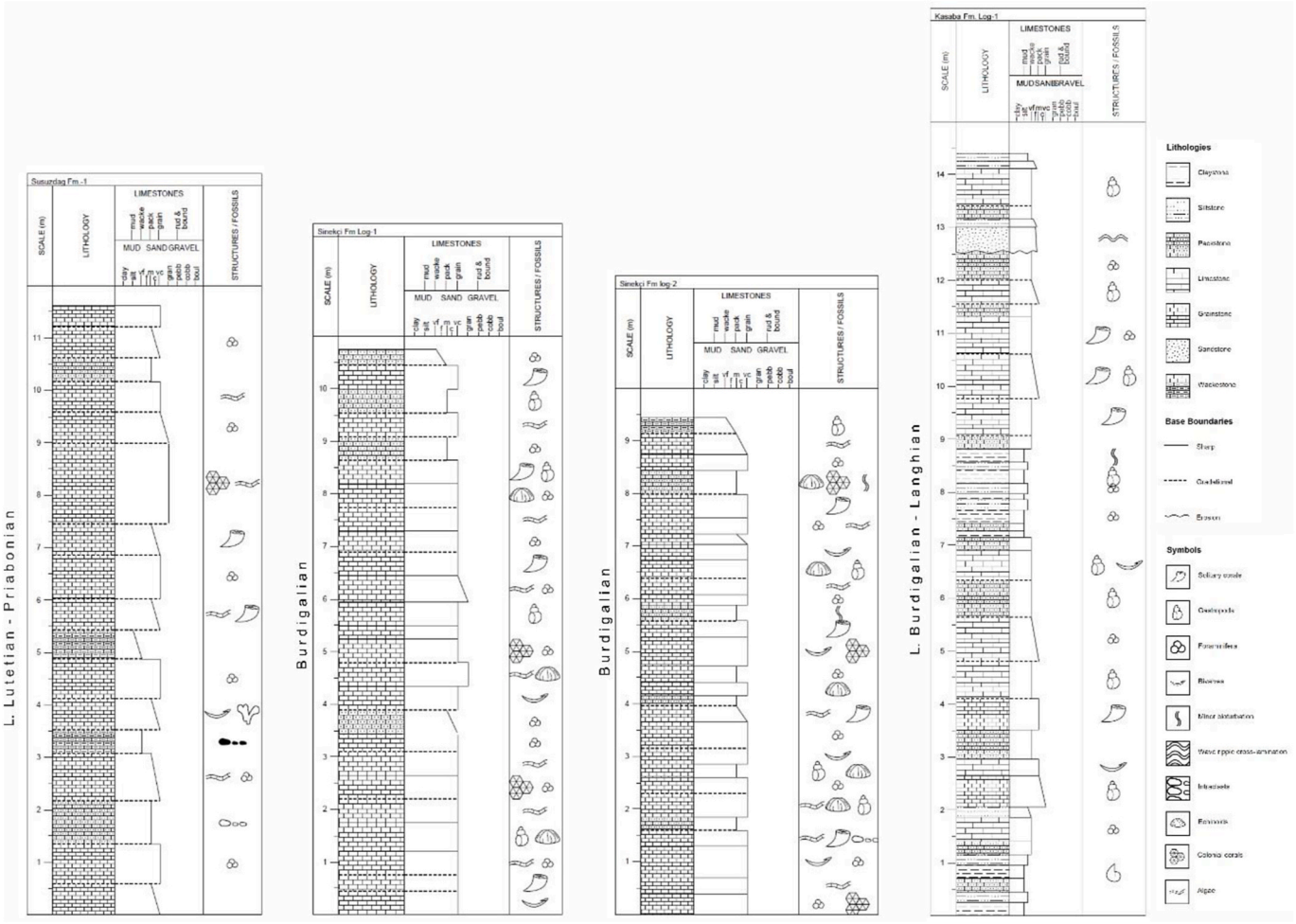


Fig. 4. Measured sedimentological logs of the Susuzdağ, Sinekçi and Kasaba formations exposed in the Kasaba Basin.

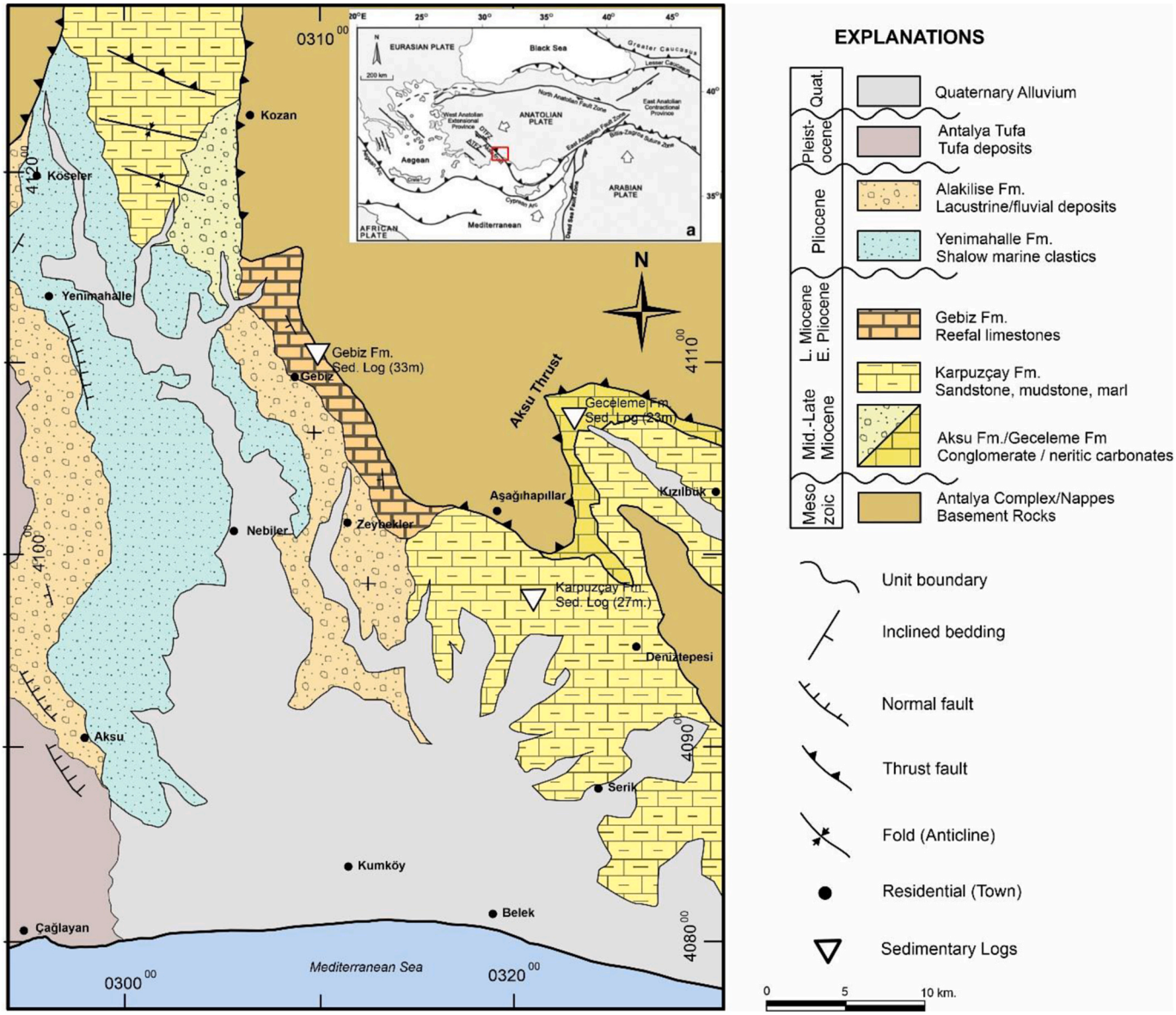


Fig. 5. Simplified geological map of the Aksu-Gebiz Basin and surrounding region (modified after Akay et al., 1985a; Akbaş et al., 2011; Üner et al., 2018).

significant strike-slip motion (Yağmurlu et al., 2005; Kaymakcı et al., 2017; Alçiçek et al., 2017). This zone also serves as a transition zone between the Anatolian Plateau, which is moving westward and uplifting, and the Western Anatolian region, which is moving southwestward and rotating counterclockwise (Schildgen et al., 2012; Çiner et al., 2015). However, it is important to note that these studies are not based on GPS data. For GPS-based studies on regional tectonics, see Reilinger et al. (2006), who used GPS measurements to provide a detailed analysis of plate motion and crustal deformation in the Eastern Mediterranean region.

The Aksu-Gebiz Basin has been developing unconformably over the Antalya, Beyşehir-Hoyran-Hadım, and Lycian nappes since the late Cenozoic (Fig. 5). This basin consists of three closely related sub-basins: Aksu, Köprüçay, and Manavgat Sub-basins (Karabıyıkoğlu et al., 2005a, 2005b; Yılmaz et al., 2024). The main tectonic elements dividing these three basins are the Kırkkavak Fault and the Aksu Ridge, which face west and southwest, respectively (Dumont and Kerey, 1975; Akay et al., 1985b; Çiner et al., 2008; Poisson et al., 2011; Hall et al., 2014).

Four main stages stand out in the tectonic-stratigraphic evolution of the Aksu Basin. Especially, French researchers have provided valuable insights into the Aksu phase by offering new data on the age of the Aksu Thrust and discussing the late Cenozoic evolution of the Aksu Basin in the Isparta Angle region (Poisson, 1977; Flecker et al., 1995, 1998; Poisson et al., 2003, 2011). Their research indicates that the Aksu Basin developed as an elongated N-S graben, filled with terrestrial and marine deposits, including coral reefs formed from the erosion of the Lycian nappes and their basement during Langhian, Serravallian, and Tortonian times. The reactivation of normal faults along the basin's western margin and the continuous uplift of neighboring continental areas, marking the onset of the Aksu Thrust, have significantly influenced the basin's geometry. The first stage is a regional compression stage with an NW-SE orientation that led to the settlement of the Lycian nappes in the Langhian. This stage induced the formation of the basin and the initial deformation. This stage is followed by a dominant NW-SE extensional stress regime between the Langhian and the Messinian. This regime is terminated by the NE-SW compression stress regime, also referred to the Aksu Stage (Üner et al., 2018). The most recent neotectonic period is characterized by a NE-SW extensional regime starting in the late Pliocene (Üner et al., 2015).

The Aksu-Gebiz Basin encompasses an area of approximately 2000

km^2 and is bounded by the Bey Dağları Mountains Platform carbonates to the west and the Aksu Fault to the east (Fig. 2). The basin fill starts unconformably overlying the basement with the Geceleme Formation to the east and, intermittently, the lateral transitional Aksu Formations to the west. During the Langhian-Serravallian, the Aksu Formation and the Geceleme Formation are almost contemporaneously deposited, forming five different Delta Fans that are fed from the north (Kapıkaya Fault Zone), west (Karadağ, Kargı, and Bucak Fault Zones), and east (Kozan Fault Zone) of the basin. In the western and northwestern parts of the basin, the Aksu Formation consists of thick-bedded, consolidated conglomerates, while in the east, the Geceleme Formation, consisting of shallow marine carbonates and conglomerates deposited in a shallow marine environment, passes into the Serravallian-Tortonian-aged Karpuzçay Formation, which is characterized by fine-grained sediments (Fig. 3). The upper levels of the Karpuzçay Formation, composed of fine-grained sediments, pass conformably/upward into patchy reefs (Gebiz Formation) (Karabıyıkoğlu et al., 2005a, 2005b). During the Messinian Salinity Crisis, the basin experienced a transition from shallow marine to terrestrial environments. After the crisis, rising sea levels restored marine conditions in the southern Aksu Basin, whereas the northern regions (Eskiköy Formation) remained terrestrial. Sedimentary units deposited during this time were irregularly covered by the shallow marine Messinian-Zanclean-aged Yenimahalle Formation which consists of lithologies such as neritic limestone marl and siltstone in the southern part of the basin (Fig. 3b) (Şenel, 1997; Poisson et al., 2003; Çiner et al., 2008). The unit begins with sandy clayey levels at the base and continues upward with minor marl-clayey levels, followed by medium-to thick-bedded, coral-rich, oncolitic, algal, and lamellar branched levels. These units transition from lacustrine deposits to the fluvial Pliocene Alakilise Formation, which consists of thick-bedded conglomerates, lacustrine limestones, and siltstones (Poisson et al., 2003). The uppermost basin fill comprises Quaternary Antalya tufa and alluvium (Koşun, 2012) (Fig. 3).

The measured sedimentary logs from the Aksu-Manavgat Basin (Fig. 6) record a dynamic depositional history from the Serravallian to the Messinian, illustrating a transition from fine-grained siliciclastic sedimentation to carbonate-dominated reefal environments. The Karpuzçay Formation, representing the oldest unit in the succession, is primarily composed of fine-grained sediments, including claystones and siltstones, suggesting deposition in a low-energy outer shelf to offshore environment. The presence of thin interbedded sandstones with ripple cross-lamination indicates occasional higher-energy pulses, possibly linked to storm events or minor turbidity currents. Upward in the sequence, the formation transitions conformably into patchy reefal limestones, marking a shift to a shallower, more oxygenated marine setting with enhanced carbonate production. The overlying Geceleme Formation consists of alternating shallow marine carbonates and conglomerates, reflecting fluctuating energy conditions. The conglomerates, with clast-supported textures and erosive basal contacts, suggest channelized deposits formed by episodic high-energy currents, likely in a shoreface or tidal inlet setting. Sedimentary structures such as trough cross-bedding and imbricated clasts within these conglomerates further support deposition under strong hydrodynamic conditions, possibly influenced by sea-level fluctuations or tectonic activity. The Gebiz Formation, of Messinian age, caps the sequence with well-developed reefal limestones and shelf carbonates, signifying the establishment of a high-energy, shallow marine carbonate platform. The reefal facies contain abundant coral and algal frameworks, indicating a warm, nutrient-rich environment with minimal siliciclastic input. The overall stratigraphic trend reflects a regressive evolution, where the basin transitioned from a fine-grained siliciclastic-dominated system toward an extensive carbonate platform, driven by a combination of tectonic uplift, sea-level fluctuations, and changes in sediment supply dynamics.

Previous biostratigraphic studies have provided essential age constraints for the sedimentary sequences of the Kasaba and Aksu-Gebiz Basins, offering a foundation for evaluating the new strontium isotope

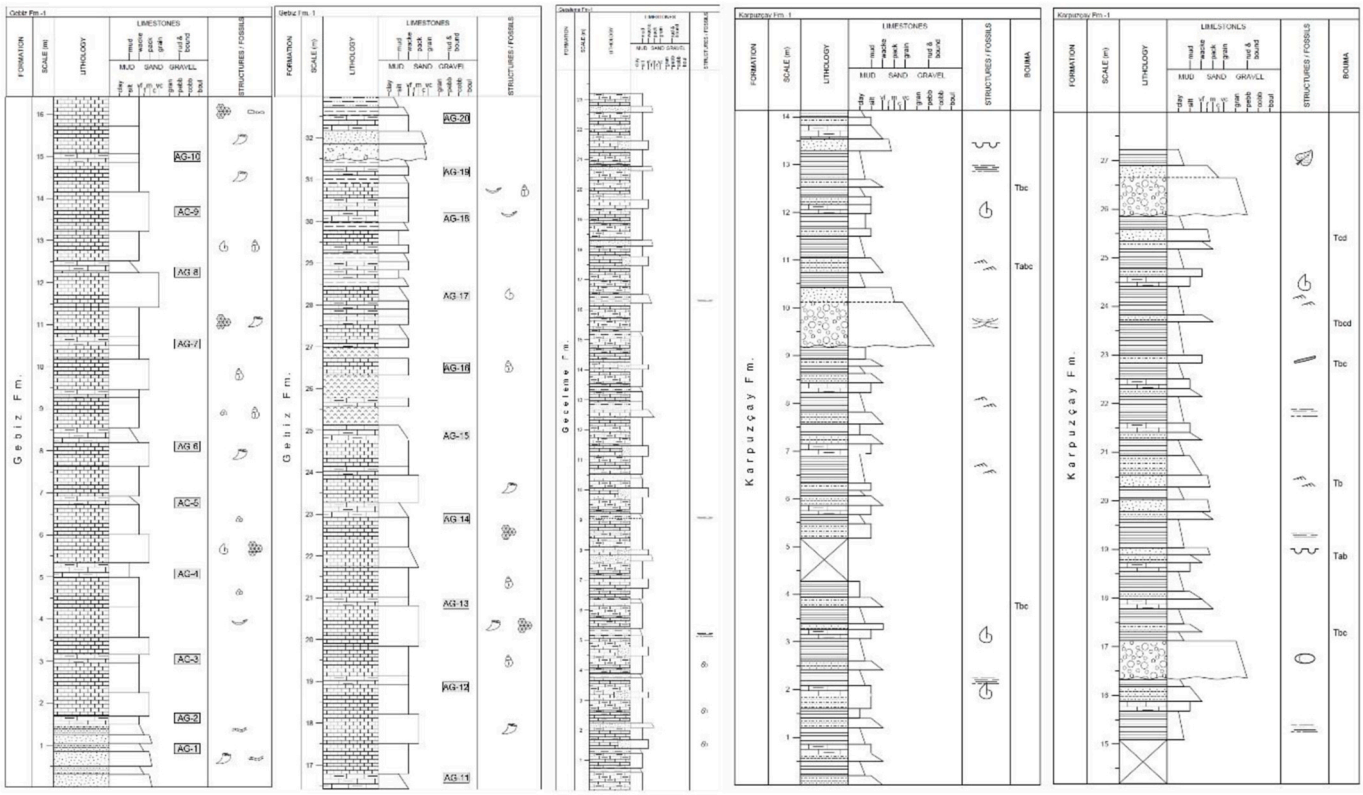


Fig. 6. Measured sedimentological logs of the L. Miocene-E. Pliocene reefal carbonates of the Gebiz Formation, Mid.-Late Miocene Geceleme and Karpuzçay formations exposed in the Aksu-Gebiz Basin.

data (Table 1). In the Kasaba Basin, the Kasaba Formation has been dated to the Serravallian-Tortonian based on foraminiferal assemblages and nannofossil biostratigraphy (Önalan, 1979; Hayward, 1982). The overlying Sinekçi Formation is characterized by Langhian and Burdigalian-Langhian deposits, supported by micropaleontological evidence (Şenel et al., 1994). Additionally, the Susuzdağ Formation has been assigned a Middle Miocene age, primarily based on mollusk and foraminiferal data (Tunoğlu and Bilen, 2001). In the Aksu-Gebiz Basin, the Geceleme Formation spans the Burdigalian-Langhian interval, as indicated by planktonic foraminifera and calcareous nannofossils (Özgül, 2002). The Aksu and Karpuzçay formations have been biostratigraphically correlated with the Langhian-Serravallian based on the presence of key benthic and planktonic foraminiferal species (Özgül, 2002). The Gebiz Formation, representing one of the youngest deposits in the basin, has been assigned a Middle Miocene age based on larger foraminifera and nannofossil assemblages (İslamoğlu, 2004). These biostratigraphic age assignments establish a chronological framework for interpreting the depositional history of both basins. Strontium isotope stratigraphy offers an independent approach to refine these constraints and enhance the temporal resolution of the Neogene sequences.

3. Methods

For Sr isotope and biostratigraphy studies, detailed sedimentary logs were recorded in sections (Figs. 4 and 6) where units exhibited good exposure and displayed characteristic features in the field. As part of the fieldwork, a 1:100,000 scale basic geological map of the region was produced. For biostratigraphic studies, 1-m interval bulk samples were collected from base to top of the units and stored in sample bags appropriately. Simultaneously, samples were also collected from unaltered and carbonate-rich levels for Sr isotopic analyses. Details of the procedures for biostratigraphy and Sr isotope studies conducted in the laboratory are summarized below.

Table 1
Summary of the available relevant biostratigraphic age data for the Miocene units exposed in the Kasaba and Aksu-Gebiz Basins.

	Unit	Age	Reference
KASABA BASIN	Kasaba Formation	Serravallian-Tortonian	Önalan (1979), Hayward (1982)
		Langhian	Şenel et al. (1994)
		Burdigalian-Langhian	Tunoğlu and Bilen (2001)
		Middle Miocene	İslamoğlu (2004)
	Sinekçi Formation	Early Miocene	Önalan (1979), Bölükbaşı and Yoldemir (1982)
		Burdigalian	Şenel et al. (1994), Tunoğlu and Bilen (2001)
	Susuzdağ Formation	Lutetian-Priabonian	Şenel et al. (1994), Tunoğlu and Bilen (2001)
AKSU - GEBİZ BASIN	Gebiz Formation	Messinian	Akay et al. (1985a), Poisson et al. (2003), Wasoo and Koç (2021)
		Late Miocene/ Pliocene	Poisson (1977)
		Tortonian	Glover and Robertson (1998)
	Karpuzçay Formation	Tortonian-Messinian	Karabıyıkoğlu et al. (2000)
		Late Langhian-Tortonian	Yılmaz et al. (2024)
		Late Burdigalian - Tortonian	Akay et al. (1985a)
	Aksu Formation	Serravallian-Tortonian	İslamoğlu (2002)
		Tortonian	Yılmaz et al. (2024)
		Late Oligocene-Tortonian	Akay et al. (1985a)
	Geceleme Formation	Langhian-Early Serravallian	Akay et al. (1985a); İslamoğlu (2002)
		Late Langhian-Serravallian	Karabıyıkoğlu et al. (2000); Çiner et al. (2008)

3.1. Paleontological analysis

A total of 30 samples were collected from the KM and KE sections in the Kasaba (Kaş) region, and 19 samples were obtained from the GA section in the Gebiz (Aksu) region, yielding a total of 49 samples. The samples underwent a laboratory washing process to extract the foraminifera contained within them. Each sample, weighing 200 g, was separated and left to stand for at least 24 h in hot water and 15 % diluted hydrogen peroxide (H_2O_2). The fragmented residues were then washed through sieves of 0.25 mm, 0.50 mm, and 1 mm, and after drying, they were placed into sample bags. The foraminifera contained in the samples from sections KE, KM, and GA were separated using a needle under a binocular microscope (Nikon-SMZ745T) at Kütahya Dumlupınar University and collected on microfossil slides. For the identification of planktonic foraminifera, the works of Kennett and Srinivasan (1983), Iaccarino (1985), Iaccarino et al. (2007), Fox and Wade (2013), and the website https://www.mikrotax.org/pforams/cenozoic were used. For the identification of benthic foraminifera, the work of Loeblich and Tappan (1988) was utilized. The planktonic and benthic foraminifera collected on the microfossil slides were counted, and their abundances in the samples were determined according to the number of individuals. The abundance categories are as follows: rare (1–9 individuals), few (10–20 individuals), common (21–50 individuals), abundant (51–100 individuals), and very abundant (>100 individuals). These categories were used to determine the abundances of benthic foraminifera genera and planktonic foraminifera species in the samples. The selected planktonic and benthic foraminifera were coated with gold and their images were captured using a scanning electron microscope at Kütahya Dumlupınar University Advanced Technologies Center.

3.2. Sr isotope geochronology

Thin sections of limestone and clayey limestone collected from the field were prepared at the Department of Geological Engineering, Çukurova University. These sections underwent initial examination using a binocular microscope with polarized light (Kyowa). Subsequently, they were further scrutinized using an optical microscope equipped for both transmitted and reflected light (Leica DMEP microscope at Çukurova University). Among the most commonly utilized classifications are those proposed by Folk (1959) and Dunham (1962). Strontium isotope geochemistry experiments were conducted on five samples at the Radiogenic Isotope Laboratory of the Middle East Technical University (METU) Central Laboratory in Ankara, adhering to the precise methods and conditions outlined by Köksal et al. (2017). These procedures encompassed weighing, chemical dissolution, and chromatographic processes conducted in meticulously maintained cleanroom conditions meeting class 100 standards, employing ultrapure chemicals and water.

4. Results

4.1. Paleontology

4.1.1. Description of the key sections

4.1.1.1. KM sections. This section from the Kasaba Formation, from the base up to 24 m (KM1-KM12), did not yield any fossil evidence. Beginning from 26. meters, KM13 and KM14 samples, which contain very sparse fossil content (1 %), revealed the presence of a small number (15) of poorly preserved planktonic foraminifera for the first time. In these samples, where *Orbulina suturalis* is more abundant compared to

other species, it was determined that species belonging to the genera *Dentoglobigerina*, *Trilobatus trilobus* and *Globoquadrina dehiscens* are less common (Fig. 7). In the KM15 sample, taken from the 30. meter mark of the section, which has a very rich fossil content (90 %), it was observed that the entire community is consists of planktonic foraminifera. Particularly, *O. suturalis* is the most abundant and dominant species, while *Trilobatus trilobus* is common. Additionally, *Praeorbulina circularis*, *Praeorbulina curva*, and *Trilobatus immaturus* have increased but are present in low quantities within the community. In samples KM16-KM18 (between 32m. and 36m.), where fossil content is very low (1 %), there are only a few individuals of the *Orbulina suturalis* species from very poorly preserved planktonic foraminifera, and other identified species are very rare. In samples KM19 and KM20 taken from 38. meters onward, fossil content is very abundant (95 %), with almost the entire assemblage composed of planktonic foraminifera. *Orbulina suturalis* (Figs. 10 and 9) is very abundant (>100 individuals) in these samples, with *Globoquadrina dehiscens* (Figs. 8 and 9) and *Dentoglobigerina venezuelena* species also becoming abundant (51–100 individuals) in the last sample (KM20). In this section dominated by planktonic foraminifera, small benthic foraminifera such as *Ammonia* sp., *Cibicidioides* sp., *Elphidium* sp., *Heterolepa* sp., and *Lenticulina* sp., which reflect a shelf environment, have been observed very rarely, with only one or two individuals. In the detailed biostratigraphic studies conducted on the KM section, a total of 9 genera and 23 species of planktonic foraminifera have been identified (Fig. 7). *Orbulina suturalis* shows variability in abundance across samples, being abundant to very abundant in some (KM15, KM19, KM20) and less abundant in others (KM13, KM16-KM18). The stratigraphic distribution of the other identified genera and species has also been utilized in the interpretation.

4.1.1.2. KE sections. When examining the fossil assemblage from the 20-m measured section of the Sinekçi Formation, it was observed that nearly the entire assemblage consists of planktonic foraminifera, with very few small benthic foraminifera (only 1 or 2 individuals) are present (Fig. 8). From the first sample to the last one at 20 m (KE10), species such as *Orbulina suturalis* and those from the genera *Dentoglobigerina* (*D. altispira, D. globosa, and D. venezuelana*) as well as *Trilobatus trilobus* were found to be highly abundant (>100 individuals) (Fig. 8). Meanwhile, species such as *Dentoglobigerina baroemoenensis*, *Globoquadrina dehiscens*, and *Trilobatus immaturus* were common (51–100 individuals),

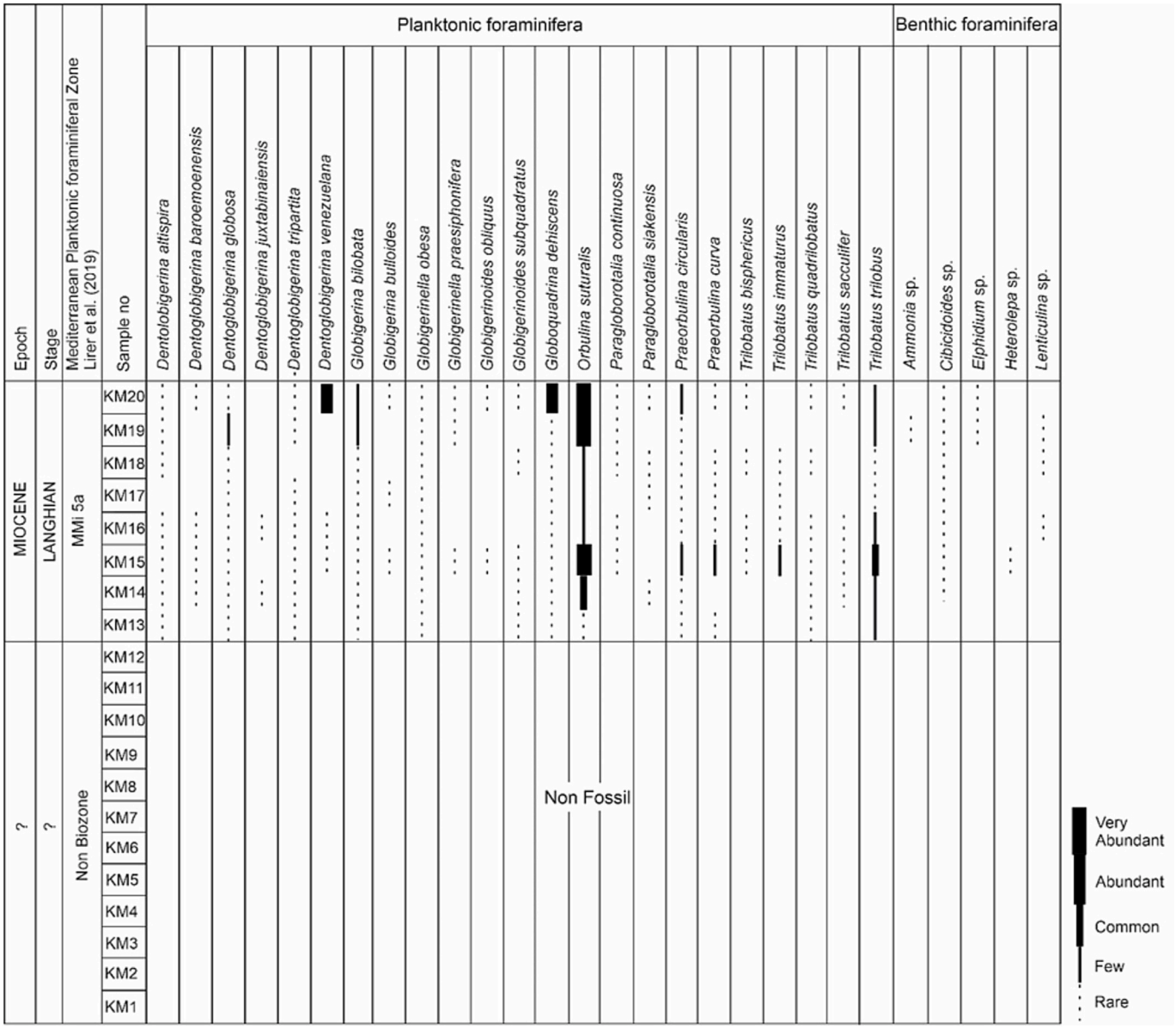


Fig. 7. Planktonic-benthic foraminiferal abundance distribution of the KM section.

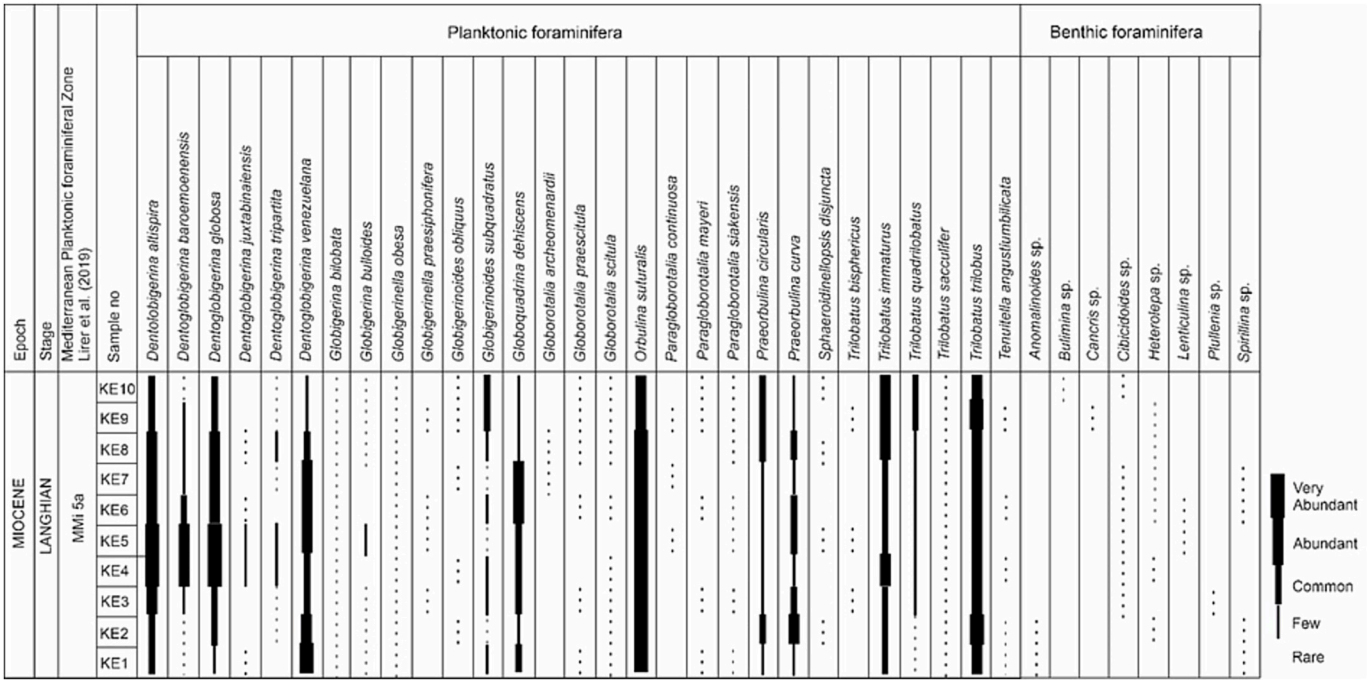


Fig. 8. Planktonic-benthic foraminiferal abundance distribution of the KE section.

and *Praeorbulina circularis* and *P. curva* were widespread (21–50 individuals), as shown in Figs. 9–10. Additionally, species such as *Globorotalia archeomenardii*, *Globorotalia praescitula*, *Globorotalia scitula*, *Paragloborotalia mayeri*, and *Paragloborotalia siakensis* were rarely observed (1–9 individuals) (Figs. 8 and 10). In this section, almost entirely dominated by planktonic foraminifera, small benthic foraminifera, including *Anomalinoides* sp., *Bulimina* sp., *Cancris* sp., *Cibicidoides* sp., *Heterolepa* sp., *Lenticulina* sp., *Pullenia* sp., and *Spirillina* sp. were found in very low numbers (1–3 individuals). In the studied section, 29 planktonic foraminiferal species have been identified, belonging to the genera *Dentoglobigerina*, *Globigerina*, *Globigerinella*, *Globigerinoides*, *Globoquadrina*, *Globorotalia,* *Orbulina*, *Paragloborotalia*, *Praeorbulina*, *Sphaeroidinellopsis*, *Trilobatus*, and *Tenuitella* (Fig. 8).

4.1.1.3. GA sections. The section was measured as 38 m from the Karpuzçay Formation, and 19 samples were studied. In sample GA1, it was determined that the fossil content was low (10 %), the clastic content was high, and planktonic foraminifera were abundant and dominant (99 %) and moderately well-preserved. Among the small benthic foraminifera, 10 individuals of *Elphidium* sp., 12 individuals of *Lenticulina* sp., 2 individuals of *Planulina* sp., and a few individuals from *Bulimina* sp., *Nonion* sp., *Cibicidoides* sp., *Heterolepa* sp., pelecypods, and gastropods were observed. Notably, in this assemblage, the species *Orbulina universa* was abundant (51–100 individuals); *Orbulina suturalis*, *Globigerinoides obliquus*, and *Trilobatus trilobus* were common (21–50 individuals), whereas *Globigerinoides extremus*, *Globigerina bilobata*, *Trilobatus immaturus*, and *Sphaeroidinellopsis seminulina* were less abundant (10–20 individuals) (Fig. 11). In samples GA2, GA3, and GA4, taken from the 2 nd m to the 6th meter of the section, the fossil content increased to 70 %, and planktonic foraminifera were abundant and dominant. The number of individuals of *Elphidium* sp. in sample GA2 was 7, which decreased to 3 in GA3, while the number of *Lenticulina* sp. increased in these samples (15 individuals). Particularly in sample GA4, it was observed that *O. universa* was very abundant (>100 individuals), *Trilobatus trilobus* was abundant (51–100 individuals), *Globigerinoides extremus* and *Globigerinoides obliquus* were decreasing, and small benthic foraminifera such as *Elphidium* sp. were absent, while *Siphonina* sp., *Lenticulina* sp., and *Planulina* sp. increased (approximately 15 individuals) (Fig. 11). In sample GA5, taken from the 8th meter of the section, it was observed that the fossil content decreased (25 %) while the clastic content increased.

In the sample GA9, taken from the 16th meter, the fossil content was low (30 %), the clastic ratio was high, and planktonic foraminifera made up 99 % of the assemblage. This sample contained *Lenticulina* sp. (15 individuals), *Elphidium* sp. (7 individuals), 3 individuals each of *Uvigerina* sp., *Bulimina* sp., and *Planulina* sp., and one individual each of *Quinqueloculina* sp., Ammonia sp., pelecypods, and gastropods. In contrast, samples GA6, GA7, GA8, GA10, and GA11 showed higher fossil content (60–70 %) and lower clastic content. Similar to previous samples, the fossil assemblage in these samples was dominated by abundant and dominant planktonic foraminifera (99 %). Among the small benthic foraminifera identified in these samples, *Lenticulina* sp. (22–23 individuals), *Bulimina* sp. (10–15 individuals), and *Siphonina* sp. (10–15 individuals) were more abundant compared to other small benthic foraminifera. Additionally, at the 20th meter of the section, in sample GA11, *Globigerinoides extremus* was observed for the first time in common numbers (21–50 individuals). Alongside *Lenticulina* sp. (22 individuals) and *Elphidium* sp. (7 individuals), 6 individuals of *Nonion* sp. were identified for the first time in the section. In sample GA12, taken from the 24th meter, the fossil content reached its highest level in section (100 %), with planktonic foraminifera making up nearly the entire assemblage. As in previous samples, the most abundant species in GA12 was again *Orbulina universa*. Small benthic foraminifera in GA12 included *Lenticulina* sp. (12 individuals) and *Elphidium* sp. (3–4 individuals). From the base of the section (GA1) to the 24th meter (including GA12), the fossil assemblages in these samples were dominated by moderately to well-preserved planktonic foraminifera (Figs. 11 and 12). In these samples (GA1-GA12), *Orbulina universa* was very abundant to abundant, while species such as *Orbulina suturalis*, *Trilobatus trilobus,* and *Globigerinoides obliquus* were occasionally abundant and widespread. Other species (*Globigerinoides extremus, Globigerina bilobata, Sphaeroidinellopsis seminulina, Trilobatus immaturus, Trilobatus quadrilobatus, Trilobatus sacculifer*) were less common, and *Globigerinita uvula*, *Globigerinella obesa*, *Neogloboquadrina acostaensis*, *Neogloboquadrina atlantica*, and species from the genera *Sphaeroidinellopsis* (*S. kochi* and *S. sphaeroides*) were rare.

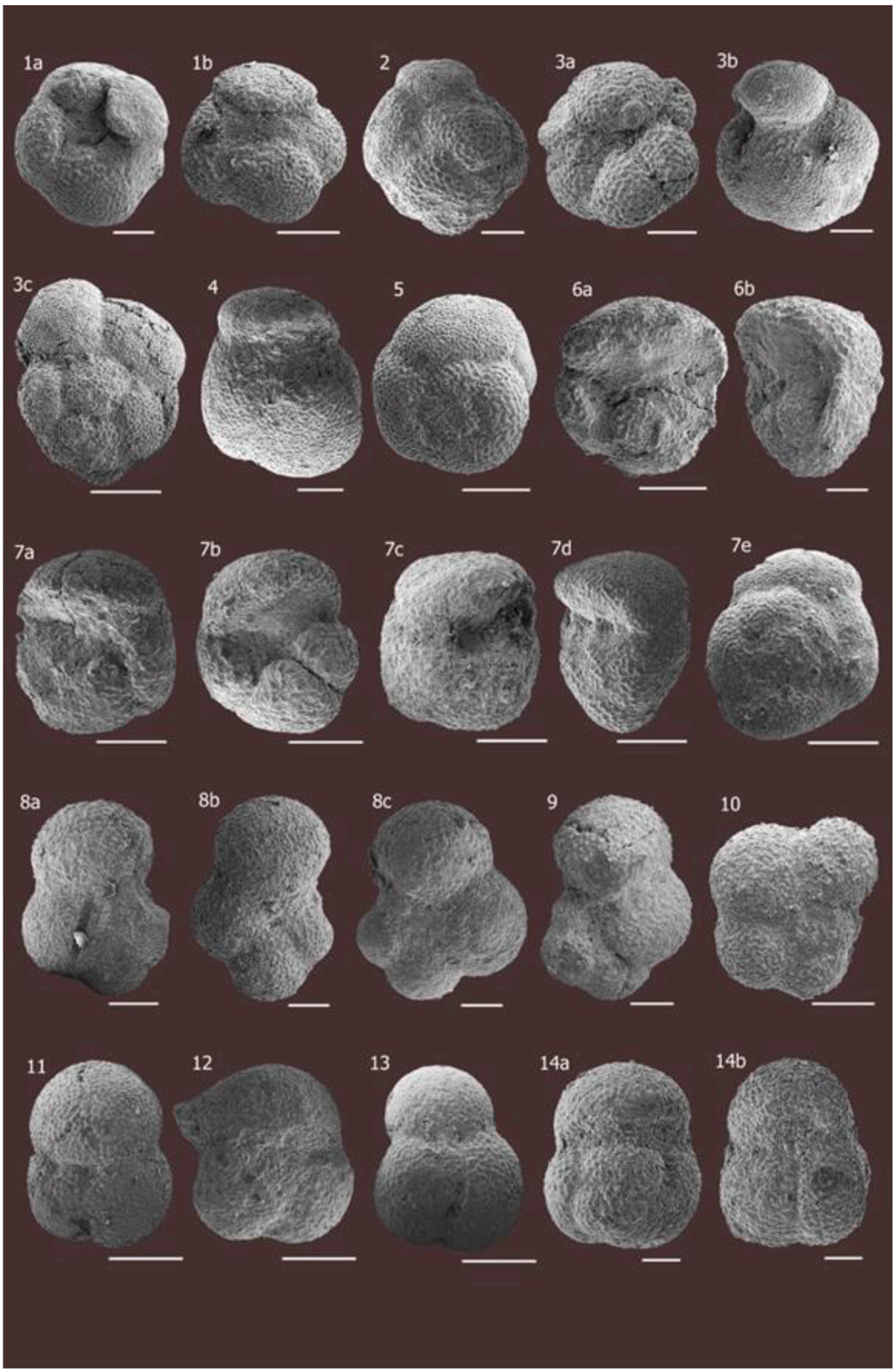


Fig. 9. SEM images of planktonic foraminifera described in KE section. 1a-b. *Dentoglobigerina venezuelana* (Hedberg), **a**; umbilical view, KE section, sample no:9, **b**; umbilical view, KE section, sample no:3, **2**. *Dentoglobigerina altispira* (Cushman and Jarvis), spiral view, KE section, sample no:5, **3a-c**. *Dentoglobigerina globosa* (Bolli), **a**; umbilical view, KE section, sample no:5, **b**. peripheral view, c. spiral view, KE section, sample no:4, **4.** *Dentoglobigerina baroemoenensis* (LeRoy), umbilical view, KE section, sample no:5, **5**. *Dentoglobigerina tripartita* (Koch), spiral view, KE section, sample no:5, **6a-b**. *Dentoglobigerina juxtabinaiensis* Fox and Wade, **a**; umbilical view, **b**; peripheral view, KE section, sample no:5, **7a-e**. *Globoquadrina dehiscens* (Chapman, Parr and Collins), **a-c**; umbilical view, **d**; peripheral view, KE section, sample no:3, **e**; spiral view, KM section, sample no:20, **8a-c**. *Globigerinella obesa* (Bolli), **a**; spiral view, KE section, sample no:7, **b-c**; umbilical view, KE section, sample no:2, **9**. *Globigerinella praesiphonifera* (Blow), umbilical view, KE section, sample no:3, **10**. *Tenuitella angustiumbilicata* (Bolli), umbilical view, KE section, sample no:6, **11**. *Trilobatus immaturus* (LeRoy), spiral view, KE section, sample no:8, **12**. *Globigerinoides obliquus* Bolli, spiral view, KM section, sample no:15, **13.** *Trilobatus quadrilobatus* (d'Orbigny), spiral view, KE section, sample no:5, **14a-b**. *Globigerinoides subquadratus* Brönnimann, **a**; spiral view, KE section, sample no:2, **b**; umbilical view, KE section, sample no:5. Scale bars: 1a, 2, 3a-b, 4, 7d, 8a-c, 9, 10,14a-b, 100 μm, 1b, 3c, 5, 6a-b, 7a-c, 7e, 11, 12, 13, 200 μm.

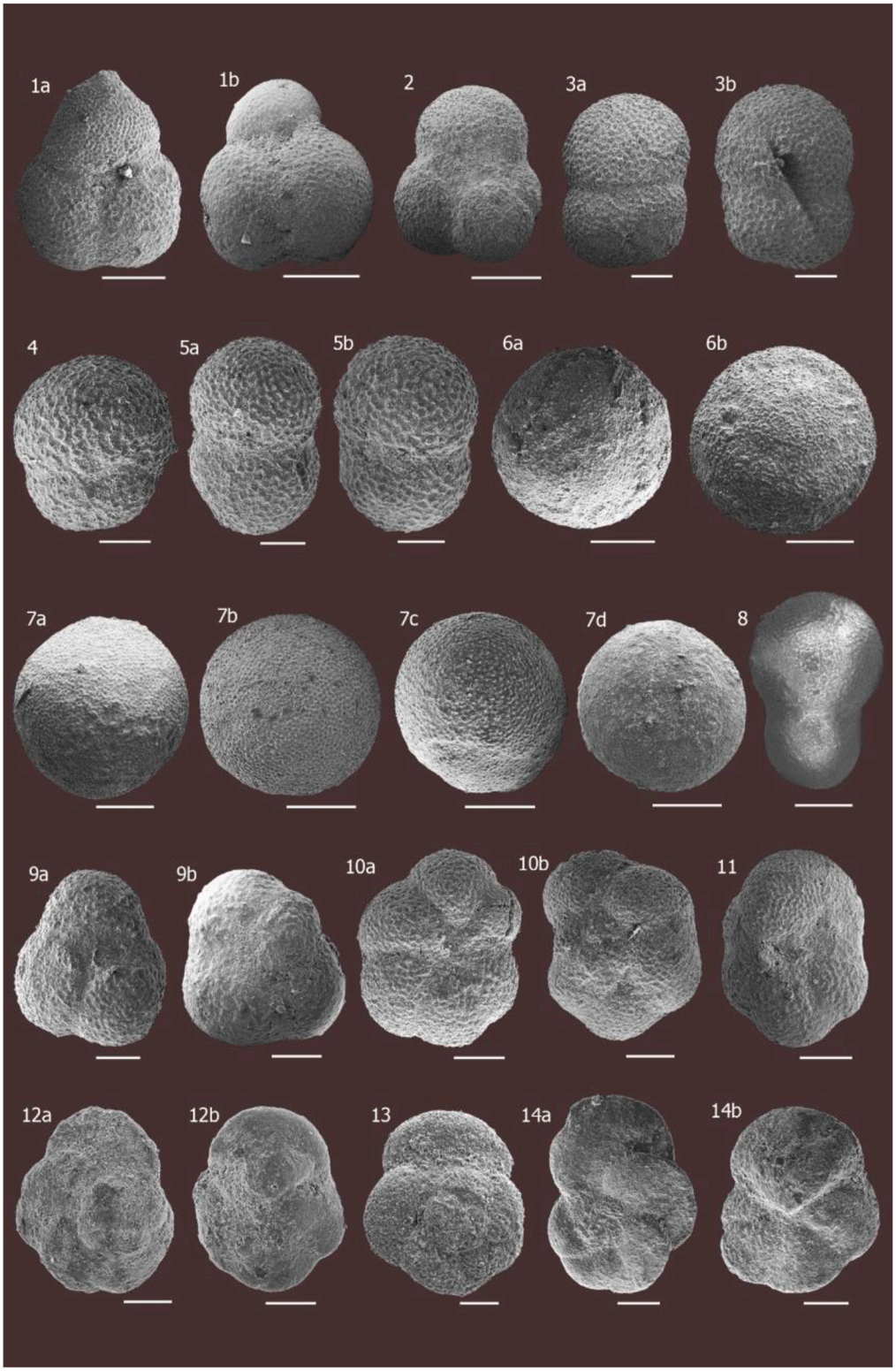


Fig. 10. SEM images of planktonic foraminifera described in KE and KM sections. 1a-b. ***Trilobatus sacculifer*** (Brady), a; umbilical view, KE section, sample no:5, b; spiral view, KE section, sample no:9, **2.** ***Globigerina bulloides*** d'Orbigny, umbilical view, KE section, sample no:9, **3a-b.** ***Trilobatus trilobus*** (Reuss), a; spiral view, KE section, sample no:1, b; umbilical view, KE section, sample no:9, **4.** ***Trilobatus bisphericus*** (Todd), umbilical view, KE section, sample no:3, **5a-b.** ***Praeorbulina curva*** (Blow), a; peripheral view, b; umbilical view, KE section, sample no:3, **6a-b.** ***Praeorbulina circularis*** (Blow), KE section, sample no:1, **7a-d.** ***Orbulina suturalis*** Brönnimann, a-c; KE section, sample no:5, d; KM section, sample no:20, **8.** ***Globigerina bilobata*** d'Orbigny, KM section, sample no:15, **9a-b.** ***Sphaeroidinellopsis disjuncta*** (Finlay), umbilical view, KE section, sample no:8, **10a-b.** ***Paragloborotalia siakensis*** (LeRoy), a; umbilical view, KE section, sample no:10, b; spiral view, KE section, sample no:1, **11.** ***Paragloborotalia mayeri*** (Cushman and Ellisor), umbilical view, KE section, sample no:6, **12a-b.** ***Globorotalia archeomenardii*** Bolli, a; spiral view, b; umbilical view, KE section, sample no:7, **13.** ***Globorotalia praescitula*** Blow, spiral view, KE section, sample no:3, **14a-b.** ***Globorotalia scitula*** (Brady), a; spiral view, KE section, sample no:1, b; umbilical view, KE section, sample no:8. Scale bars: 1a-b, 2, 6a-b, 7a-d, 8, 200 μm, 3a-b, 4, 5a-b, 9a-b, 10a-b, 11, 12a-b, 14a-b, 100 μm, 13, 50 μm.

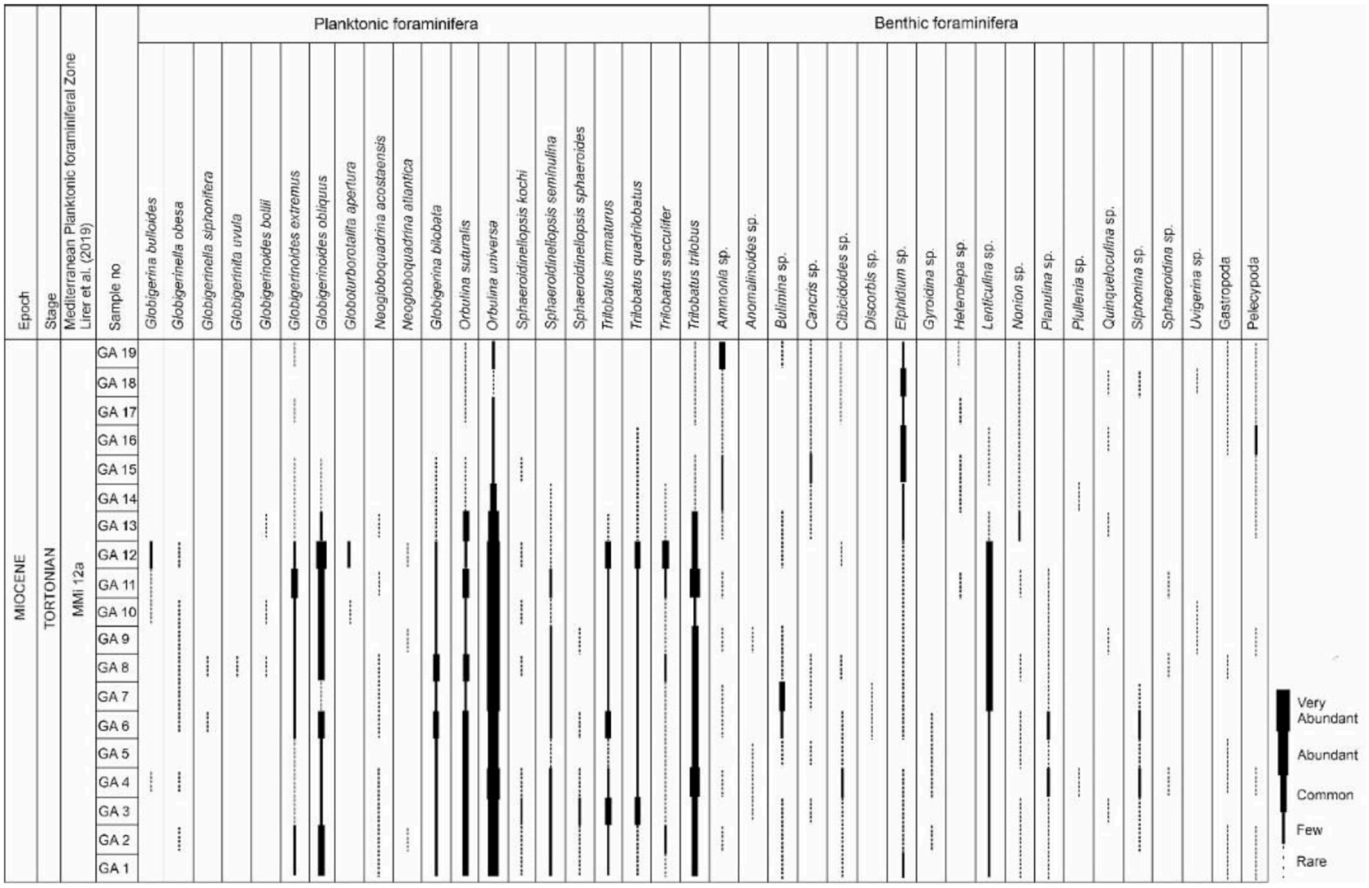


Fig. 11. Planktonic-benthic foraminiferal abundance distribution of the GA section.

In sample GA13, taken from the 26th meter, the fossil content was observed to be significantly lower for the first time in section (7 %). Along with the decrease in fossil content, the proportion of planktonic foraminifera also decreased (85 %), while the number of small benthic foraminifera began to increase (Fig. 11). *Elphidium* sp., which did not exceed 10 individuals in GA1-GA12, was counted at 15–16 individuals in GA13 for the first time. Along with *Elphidium* sp., the numbers of *Nonion* sp. and *Ammonia* sp. also increased (10–15 individuals), while the number of *Lenticulina* sp. decreased (3 individuals). Although the proportion of planktonic foraminifera decreased in GA13, *Orbulina universa* remained abundant (51–100 individuals), with *Orbulina suturalis* and *Trilobatus trilobus* being common (21–50 individuals), and other planktonic foraminifera species were less common and rare. In sample GA14, taken from the 28th meter, the fossil content decreased further (2 %), and the proportion of benthic foraminifera increased (85 %). The number of *Orbulina universa* individuals, which had been very abundant to abundant throughout the section, decreased for the first time in GA14 (10–20 individuals). The majority of the assemblage in this sample was composed of small benthic foraminifera, including *Elphidium* sp. (15 individuals), *Ammonia* sp. (10 individuals), *Cancris* sp., and *Nonion* sp. (3–4 individuals). In sample GA15, the fossil content was observed to be very low (1 %). However, *Elphidium* sp., with an increased size and number of individuals (30 individuals), became widespread for the first time in this sample. Along with *Elphidium* sp., *Ammonia* sp. (10 individuals), *Cancris* sp. (8 individuals), pelecypods (3 individuals), and *Nonion* sp. (1 individual) were also identified. In GA15, where benthic foraminifera content was high (>90 %), *Orbulina universa* was found in small numbers, and other planktonic foraminifera species (*Globigerinoides extremus*, *Orbulina suturalis*, *Trilobatus trilobus*, etc.) were rare and very rare. In the GA16 sample, which has very scarce fossil content (2 %), the proportion of small benthic foraminifera is 98 %. This sample includes 11 individuals of *Orbulina universa*, along with *Elphidium* sp. (25 individuals), *Ammonia* sp. (11 individuals), *Nonion* sp. (4 individuals), *Quinqueloculina* sp. (3 individuals), 1 gastropod, and 11 small pelecypods. The GA17 sample, taken from the 34th meter, also has very scarce fossil content (1 %), with the majority of the assemblage (99 %) consisting of small benthic foraminifera such as *Elphidium* sp. (13 individuals), Ammonia sp. (4–5 individuals), *Nonion* sp. (2 individuals), *Quinqueloculina* sp. (2 individuals), and *Cancris* sp. (1 individual), along with 3 pelecypods and 1 gastropod.

In the GA18 sample, taken from the 36th meter, with a very low fossil content (1 %), the planktonic foraminifera identified include *Orbulina universa* (8 individuals), *Orbulina suturalis* (1 individual), and *Trilobatus trilobus* (1 individual). In this sample, the assemblage is almost entirely composed of small benthic foraminifera, gastropods, and pelecypods, including *Elphidium* sp. (30 individuals), *Ammonia* sp. and *Nonion* sp. (7 individuals each), *Cibicidoides* sp. (2 individuals), *Cancris* sp., *Uvigerina* sp., *Quinqueloculina* sp. (1 individual each), 3 pelecypods, and 1 gastropod. The final sample in the section, GA19, also has very scarce fossil content (1 %). In this sample, the number of small benthic foraminifera (approximately 40 individuals) is greater than that of planktonic foraminifera (approximately 20 individuals). In this last sample of the section, *Orbulina universa* is scarce (14 individuals), and *Orbulina suturalis*, *Globigerinoides extremus*, and *Trilobatus trilobus* are rare (2 individuals each). Additionally, the number of individuals of *Ammonia* sp. has increased (22 individuals). The sample also includes *Elphidium* sp. (10 individuals), *Nonion* sp. and *Cibicidoides* sp. (4 individuals each), *Heterolepa* sp. (2 individuals), *Cancris* sp. (1 individual), 6 pelecypods, and 1 gastropod. The detailed biostratigraphic analysis conducted on the 19 samples taken from the GA section identified 9 genera and 20 species of planktonic foraminifera (Fig. 12), along with 17 genera of benthic foraminifera (Figss. 13–15). The planktonic foraminifera species

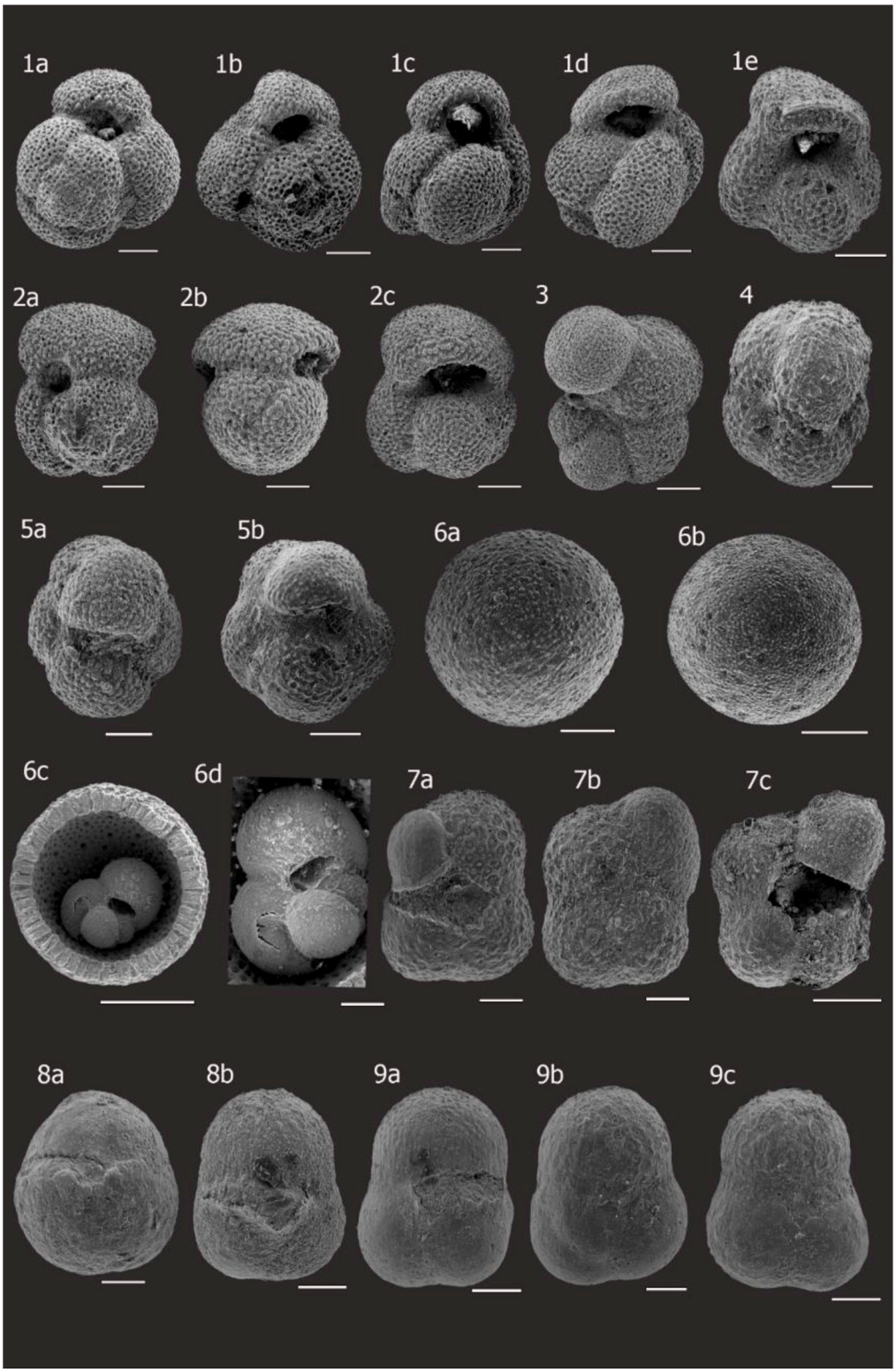


Fig. 12. SEM images of planktonic foraminifera described in GA section. 1a-e**.** *Globigerinoides extremus* Bolli and Bermúdez, a; spiral view, GA section, sample no:5, b; spiral view, GA section, sample no:8, c; umbilical view, GA section, sample no:12, d-e; umbilical view, GA section, sample no: 10, **2a-c.** *Globigerinoides obliquus* Bolli, a; spiral view, GA section, sample no:10, b; peripheral view, c; umbilical view, GA section, sample no:12, **3.** *Globigerinella siphonifera* (d'Orbigny), umbilical view, GA section, sample no:8, **4**. *Neogloboquadrina acostaensis* (Blow), umbilical view, GA section, sample no:7, **5a-b.** *Neogloboquadrina atlantica* (Berggren), a; umbilical view, GA section, sample no:9, b; umbilical view, GA section, sample no:12, **6a-d.** *Orbulina universa* d'Orbigny, c-d; internal structure, GA section, sample no:10, **7a-c.** *Sphaeroidinellopsis kochi* (Caudri), a, c; umbilical view, GA section, sample no:3, b; spiral view, GA section, sample no:8, **8a-b.** *Sphaeroidinellopsis sphaeroides* Lamb, umbilical view, GA section, sample no:3, **9a-c.** *Sphaeroidinellopsis seminulina* (Schwager), GA section, sample no:4. Scale bars: 1a-e, 2a-c, 4, 5a-b, 6a, 7a-b, 8a-b, 9a-c, 100 μm, 6b-c, 7c, 200 μm, 6d, 50 μm.

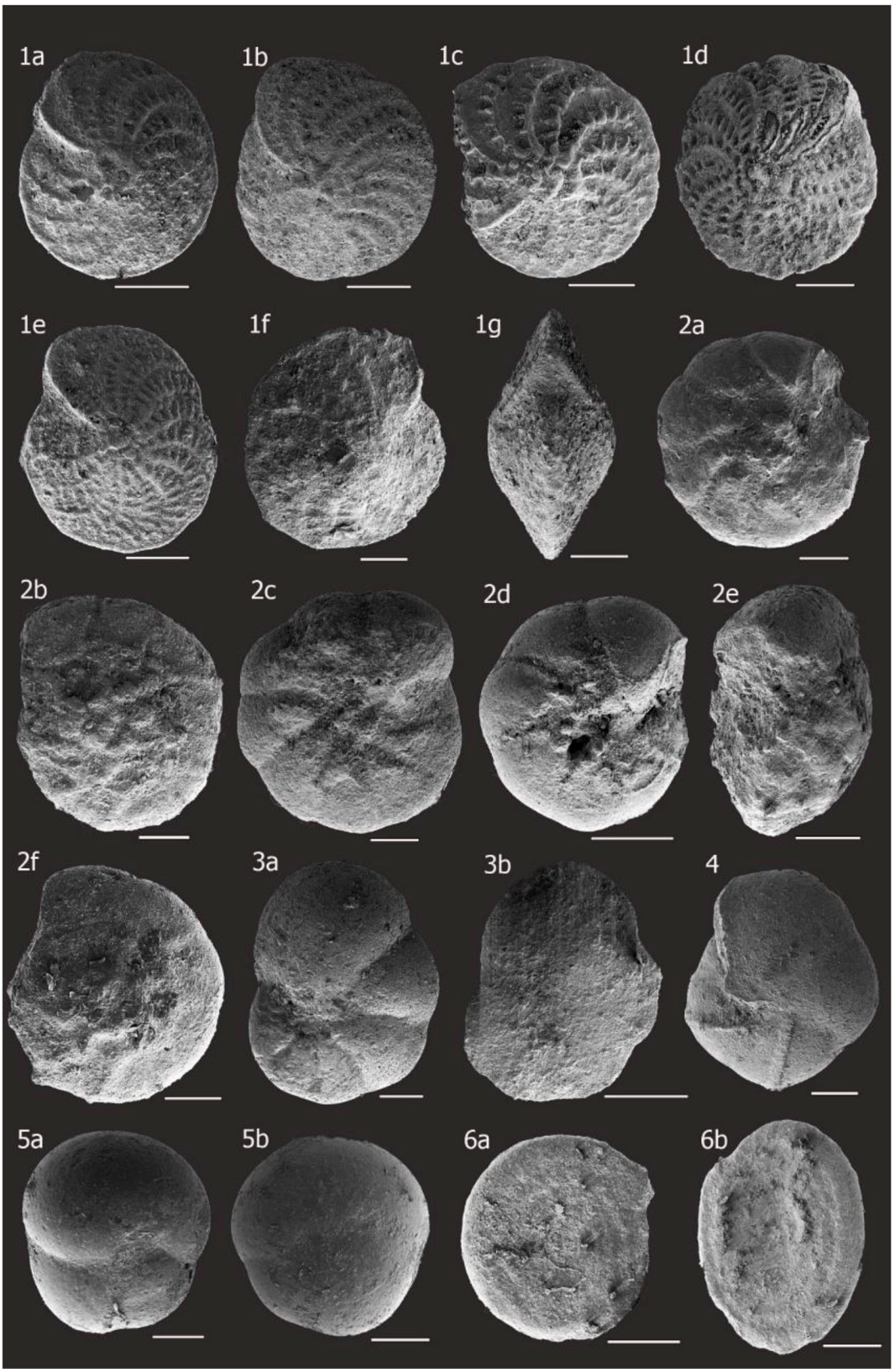


Fig. 13. SEM images of benthic foraminifera described in Aksu-Gebiz and Kasaba Basins. **1a-g.** *Elphidium* sp., GA section a; sample no:20, b; sample no:15, c,f; sample no:14, d; sample no:13, e; sample no:12, g; sample no:15, **2a-f.** *Ammonia* sp., GA section a; sample no:19, b,e,f: sample no:20, c–d: sample no:14, **3a-b.** *Cancris* sp., GA section sample no:15, **4.** *Pullenia* sp., GA section sample no: 6,**5a-b.** *Sphaeroidina* sp., GA section a; sample no:20, b; sample no:4, **6a-b.** *Spirillina* sp., KE section a; sample no:6, b; sample no:7. Scale bars: 1a-e, 1g, 2d, 3b, 6a-b, 200 μm; 1f, 2a-c, e-f, 3a, 5a-b, 100 μm.

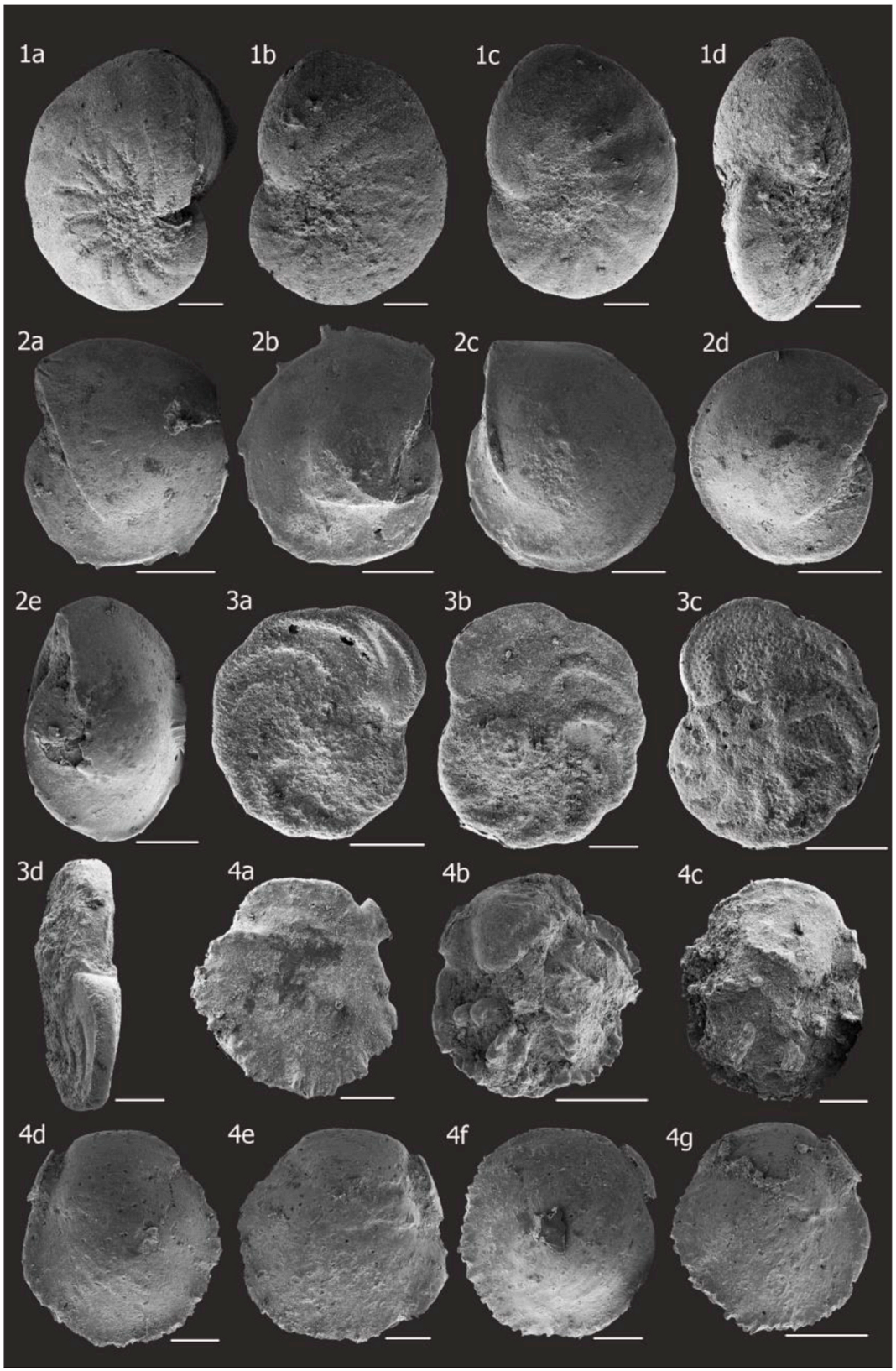


Fig. 14. SEM images of benthic foraminifera described in Aksu-Gebiz Basin. **1a-d.** *Nonion* sp., GA section sample no:13, **2a-e.** *Lenticulina* sp., GA section sample no:12, **3a-d.** *Planulina* sp., GA section sample no: 6, **4a-g.** *Siphonina* sp., GA section a, c-f; sample no: 6, b; sample no:2, g; sample no:4. Scale bars: 2a-b, 2d-e, 2d, 3a, c, 4b, g, 200 μm; 1a-d, 2c, 3b, d, 4a, 4c-f, 100 μm.

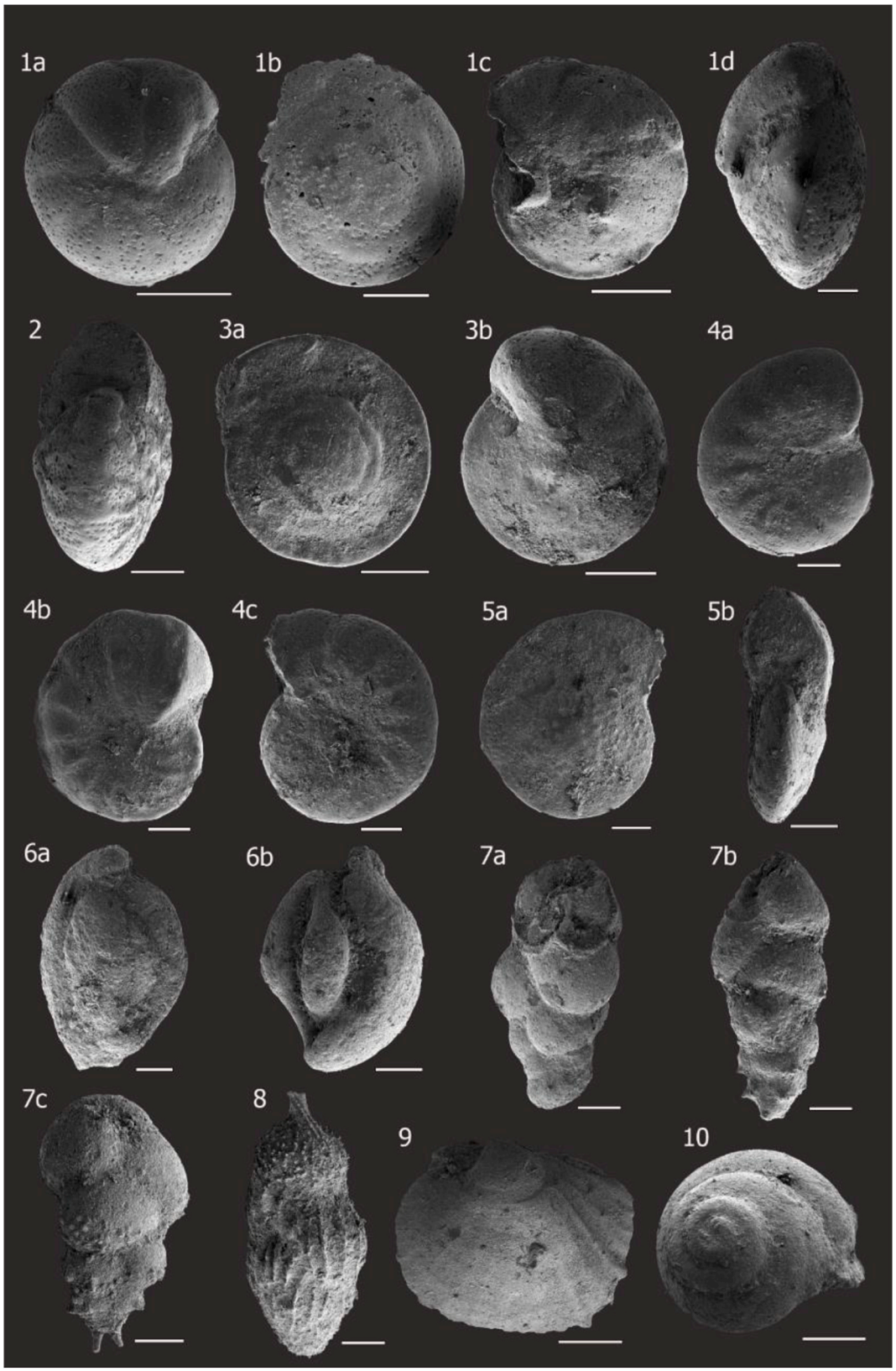


Fig. 15. SEM images of benthic foraminifera described in Aksu-Gebiz Basin. **1a-d.** *Heterolepa* sp., GA section sample no:4, **2.** *Elphidium*? sp., GA section sample no:4, **3a-b.** *Gyroidina* sp., GA section sample no:4, **4a-c.** *Anomalinoides* sp., GA section sample no:4, **5a-b.** *Cibicidoides* sp., GA section sample no:3, **6a-b.** *Quinqueloculina* sp., GA section a; sample no:17, b; sample no: 14, **7a-c.** *Bulimina* sp., GA section a-b; sample no:20, c; sample no:13, **8.** *Uvigerina* sp., GA section sample no:19, **9.** Pelecypoda GA section sample no:13, **10.** Gastropoda GA section sample no:20. Scale bars: 1a, 300 μm; 1b-c, 2, 3a-b, 8, 9, 200 μm; 1d, 2c, 4a-e, 5a-b, 6a-c, 7, 100 μm.

Globigerinoides extremus (Figs. 12 and 1a-e) was generally found in low and rare numbers from the GA1 sample to the last sample, GA19, with one instance of common occurrence in the GA11 sample. The species *Neogloboquadrina acostoensis* (Figs. 12 and 4) was found rarely throughout the section. The identified small benthic foraminifera genera, along with pelecypods and gastropods, are illustrated in Figs. 13–15.

4.1.2. Biostratigraphy

4.1.2.1. Planktonic foraminiferal biozone of Kaş/Kasaba region KM section. In the KM section, a total of 20 samples were collected, and no fossil evidence was found in the first 12 samples. In sample KM13, which has sparse fossil content, poorly preserved planktonic foraminifera were identified for the first time. Throughout the section (KM13-KM20), poorly preserved planktonic foraminifera were found to be abundant and dominant, constituting nearly the entire assemblage.

Additionally, the fossil content was notably abundant in samples KM15, KM19, and KM20. In the KM section, 9 genera and 23 species of planktonic foraminifera were identified. *Orbulina suturalis* was observed to be abundant and widespread, though sometimes less common in this section. Furthermore, the species *G. dehiscens* and *D. venezuelana* were observed to become more abundant in sample KM20. Based on the stratigraphic distribution of all described genera and species (Fig. 16), according to the Mediterranean Neogene biozone chart of Lirer et al. (2019), the lower boundary of the *Orbulina suturalis* Lineage Subzone (MMi5a) belonging to the *Orbulina suturalis-Globorotalia peripheroronda* Concurrent Range Zone (MMi5), represens the interval from the first occurrence of *Orbulina suturalis* to the last occurrence of *Globorotalia peripheroronda* in the middle Miocene (Langhian). However, due to the absence of *Orbulina universa* species in the samples, the upper boundary of this subzone could not be established. The MMi5a Subzone, identified in the Langhian (middle Miocene), corresponds to the N9 Zone in the standard zonation of Blow (1969), the M6 Zone in the subtropical zonation of Berggren et al. (1995), and Wade et al. (2011) in the tropical-subtropical zonation (Fig. 17).

4.1.2.2. Planktonic foraminiferal biozone of Kaş/Kasaba region KE section. In detailed biostratigraphic studies conducted on 10 samples from the KE section, the fossil assemblage was found to consist predominantly of moderately well-preserved planktonic foraminifera. The fossil content was abundant in this section, where 12 genera and 23 species of planktonic foraminifera were identified. According to Lirer et al. (2019), the lower boundary of the MMi5a *Orbulina suturalis* Lineage Subzone in the Langhian was determined, but the upper boundary could not be established due to the absence of the species *Orbulina universa* throughout the section (Fig. 16).

The detailed explanation and correlation related to the MMi5a Subzone, identified in the Langhian (middle Miocene), in both sections (KM and KE) from the Kaş/Kasaba region, is provided below.

4.1.2.2.1. MMi5a Orbulina suturalis Lineage Subzone. **Definition**: The interval from the first appearance of *Orbulina suturalis* to the first appearance of *Orbulina universa*.

Authors: Cita and Premoli Silva (1971–1973) in Cita (1976).

Age: Middle Miocene (Langhian); 14.56–14.36 Ma (Abdul Aziz et al., 2008)

Assemblage: *Dentoglobigerina altispira* (Cushman and Jarvis), *D. baroemoenensis* (LeRoy), *D.globosa* (Bolli), *D. juxtabinaiensis* Fox and Wade, *D. tripartita* (Koch), *D. venezuelana* (Hedberg), *Globigerina bilobata* d'Orbigny, *G. bulloides* d'Orbigny, *Globigerinella obesa* (Bolli), *Globigerinella praesiphonifera* (Blow), *Globigerinoides obliquus* Bolli, *G. subquadratus* Brönnimann, *Globoquadrina dehiscens* (Chapman, Parr and Collins), *Globorotalia archeomenardii* Bolli, *Globorotalia praescitula* Blow, *Globorotalia scitula* (Brady), *Orbulina suturalis* Brönnimann, *Paragloborotalia continuosa* (Blow), *Paragloborotalia mayeri* (Cushman and Ellisor), *Paragloborotalia siakensis* (LeRoy), *Praeorbulina circularis* (Blow), *Praeorbulina curva* (Blow), *Sphaeroidinellopsis disjuncta* (Finlay), *Trilobatus bisphericus* (Todd), *Trilobatus immaturus* (LeRoy), *Trilobatus quadrilobatus* (d'Orbigny), *Trilobatus sacculifer* (Brady), *Trilobatus trilobus* (Reuss), *Tenuitella angustiumbilicata* (Bolli).

Correlation: In the Mediterranean, during the middle Miocene, this subzone was defined as the O. suturalis Subzone by Iaccarino and Salvatorini (1982) and Iaccarino (1985), the O. suturalis Subzone (MMi5a) by Lirer et al. (2019), and the *Orbulina suturalis/Orbulina universa* (MMi5a) by Iaccarino et al. (2007). This subzone also corresponds to the O. suturalis-Globorotalia peripheroronda Zone (N9) defined by Blow (1969), the Globorotalia peripheroronda Zone (M6) defined for (sub) tropical regions by Berggren et al. (1995), and the Orbulina suturalis Zone (M6) for tropical-subtropical regions defined by Wade et al. (2011). In southern Turkey, this subzone has been identified as the Orbulina suturalis Zone in Antakya (Toker and Yıldız, 1991), Antalya (Toker, 1985; Şafak and Subaşı, 1998), Mut (Şafak and Gökçen, 1991), Adana (Nazik, 2004), and Silifke-Taşucu (Şafak et al., 2023) (Fig. 17).

4.1.2.3. Planktonic foraminiferal biozone of Aksu-Gebiz region GA section. A total of 19 samples from this section of the Karpuzçay Formation in the Gebiz (Aksu) region were studied. In the samples from GA1 to GA12, moderately well-preserved planktonic foraminifera constitute nearly the entire assemblage. In these samples, which have a high fossil content, *Orbulina universa* is particularly abundant to very abundant, while other planktonic foraminifer species are less common compared to *Orbulina universa* (see GA section figure). In sample GA13, taken from the 26. meter mark of the section, fossil content was found to be significantly reduced (7 %) for the first time, and planktonic foraminifera make up only 85 % of the assemblage. In samples GA14-GA19, where fossil content is very low (1 % or 2 %), planktonic foraminifera are still present but in small numbers. In these sparsely fossiliferous samples, the proportion of benthic foraminifera is relatively high. In the GA section, 9 genera and 20 species of planktonic foraminifera were identified (Fig. 18). Notably, *Globigerinoides extremus* was observed, though in small or rare quantities (only common in sample GA11), throughout the section from the first to the last sample (see GA section figure). Based on the stratigraphic distribution of the identified planktonic genera and species (Fig. 18), the lower boundary of the MMi12a *Globigerinoides obliquus extremus-Globorotalia suterae* Interval Subzone within the MMi12 *Globigerinoides obliquus extremus* Interval Zone in the late Miocene (Tortonian) was determined according to the Mediterranean Neogene biozone chart by Lirer et al. (2019). However, due to the absence of the species *Globorotalia suterae* in the samples from the section, the upper boundary of this subzone could not be established (Fig. 19). The MMi12a Subzone corresponds to the N16 Zone in the standard zonation of Blow (1969), the M13b Subzone in the (sub)tropical region zonation by Berggren et al. (1995), and the M13b Subzone in the tropical-subtropical region zonation by Wade et al. (2011) during the late Miocene (Tortonian). Explanations related to the identified MMi12a Subzone are provided below.

4.1.2.3.1. MMi 12a Globigerinoides obliquus extremus - Globorotalia suterae Interval Subzone. **Definition**: The interval from the first appearance of *Globigerinoides obliquus extremus* to the first appearance of *Globorotalia suterae*.

Authors: D'Onofrio et al. (1975) renamed by Iaccarino and Salvatorini (1982) and by Iaccarino et al. (2007).

Age: Late Miocene (Tortonian); 8.37–7.80 Ma (Lirer et al., 2019).

Assemblage: *Globigerina bilobata* d'Orbigny, *G. bulloides* d'Orbigny, *Globigerinella obesa* (Bolli), *Globigerinita uvula* (Ehrenberg), *Globigerinoides bollii* (Blow), *Globigerinoides extremus* Bolli and Bermúdez, *Globigerinoides obliquus* Bolli, *Globigerinella siphonifera* (d'Orbigny), *Globoturborotalita apertura* (Cushman), *Neogloboquadrina acostaensis* (Blow), *Neogloboquadrina atlantica* (Berggren), *Orbulina suturalis* Brönnimann, *Orbulina universa* d'Orbigny, *Sphaeroidinellopsis kochi*

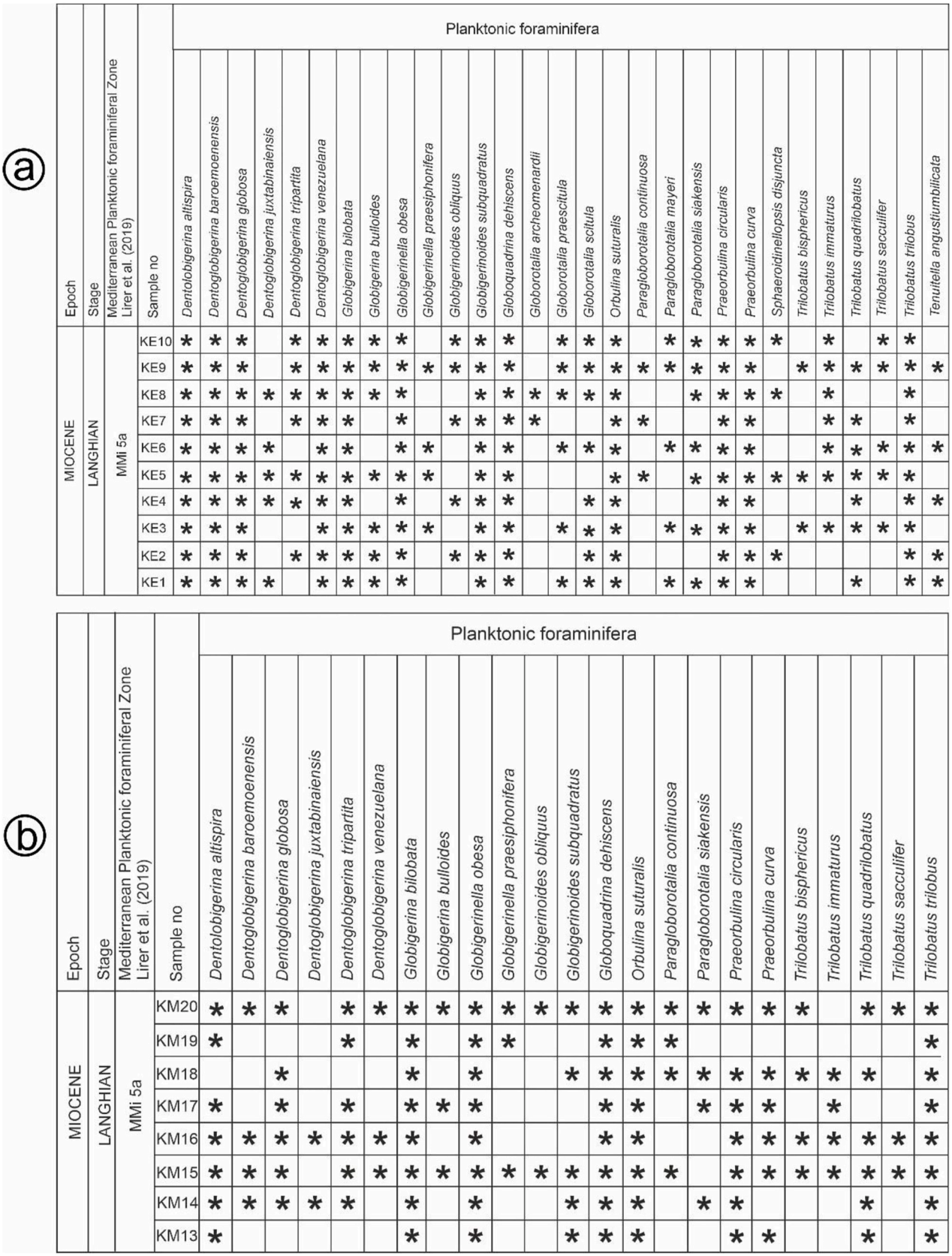


Fig. 16. Distribution and biozone of planktonic foraminiferal zones of a) KE and b) KM sections.

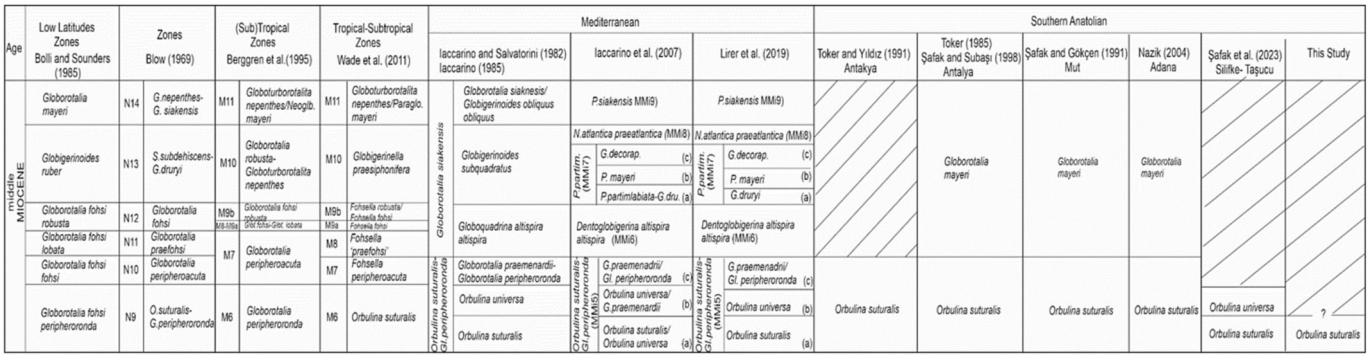


Fig. 17. Correlation table of the planktonic foraminiferal zones.

(Caudri), *Sphaeroidinellopsis sphaeroides* Lamb, *Sphaeroidinellopsis seminulina* (Schwager), *Trilobatus immaturus* (LeRoy), *Trilobatus quadrilobatus* (d'Orbigny), *Trilobatus sacculifer* (Brady), *Trilobatus trilobus* (Reuss).

Correlation: In the Late Miocene, this subzone in the Mediterranean corresponds to the Globigerinoides obliquus extremus-G. bulloideus Subzone defined by Iaccarino and Salvatorini (1982) and Iaccarino (1985), and the Globigerinoides extremus-Globorotalia suterae Subzone (MMi12a) defined by Iaccarino et al. (2007) and Lirer et al. (2019). This subzone corresponds to the G. acostaensis-Globorotalia merotumida Zone (N16) in Blow's (1969) standard zonation, to the G. extremus/Globorotalia plesiotumida-Globorotalia lenguaensis Subzone (M13b) in the (sub)tropical region zonation of Berggren et al. (1995), and to the Globorotalia plesiotumida/Globorotalia lenguaensis Subzone (M13b) in the tropical-subtropical zonation of Wade et al. (2011) (Fig. 19).

4.2. Petrography and strontium isotope analysis

4.2.1. Petrography

Through field investigations and petrographic (microfacies) examinations of 87 thin sections and five outcrop sections, we identified four primary facies: wackestone, packstone, grainstone, and mudstone within the Serravallian, Aquitanian, Tortonian, and Messinian carbonate formations studied in western Turkey (Fig. 20).

4.2.1.1. Packstone. Large to medium sized nummulites have been observed as dominant in the examined sections. These are sometimes associated with planktonic foraminifera, debris, and bivalves. This particular facies exhibits notable granulometric sorting attributed to the prevalent presence of large to medium-sized nummulites. Within the Serravallian, Aquitanian, Tortonian, and Messinian carbonate formations, sequences of grainstone/packstone rich in robust nummulites alternate with wackestone and marl layers, typically ranging in scale from 0.7 m to 3.0 m. These facies also contain occasional occurrences of iron dioxide and quartz. (Fig. 20a–d).

4.2.1.2. Grainstone. These rocks feature abundant planktonic foraminifera alongside nummulitic fragments and occasional shell remnants. The matrix exhibits a richness in organic material, nummulite debris, and sporadic silicified elements. The facies under examination is categorized as a grain-supported rock with a mud matrix content of less than 1 % (Fig. 20b–f).

4.2.1.3. Wackestone. This facies hosts infrequent planktonic foraminifera, nummulites, and shells. The wackestones are characterized by small, flat, imbricated nummulites and minor-scale cross-bedding, indicative of moderate to high depositional energy conditions. These wackestones exhibit a gray to yellow hue, accompanied by shells and small fossils, yet they lack distinct internal texture and micritic matrix (Fig. 20c–e).

4.2.1.4. Mudstone. The matrix exhibits blocky (drusy) cement locally and is intersected by calcite veins. Mudstones consist of fine-grained carbonates with a blend of silt and clay particles.

4.2.2. Strontium isotope analysis

Isotope and Elemental chemostratigraphy have been utilized in the correlation and interpretation of global events since the pioneering work of Emiliani (1955), who examined the oxygen isotope composition of foraminifers extracted from deep-sea cores. The independent variation of $^{87}Sr/^{86}Sr$ and $\delta^{13}C$ makes high-resolution chemostratigraphy an effective tool for solving geological problems. The presence of radiogenic ^{87}Sr, generated by the radioactive decay of ^{87}Rb, suggests that the $^{87}Sr/^{86}Sr$ ratio increases over time in the crust, mantle, and surface settings (e.g., Shields, 2007).

The Strontium seawater variation curve is extensively documented for the Phanerozoic era (e.g., Burke et al., 1982; Veizer et al., 1999; McArthur et al., 2001; Leckie et al., 2002; McArthur, 2010), exhibiting long-term fluctuations spanning approximately 500–550 million years from the upper Cambrian period (0.709; Montañez et al., 2000). This curve gradually decreases to its lowest point of 0.7068 at 250 million years ago, before rising again to the present-day ocean values of 0.7092 (Macdougall, 1991; McArthur et al., 2001). The utilization of Sr isotopes becomes a relatively simple and accurate approach for dating marine carbonates and calcareous fossils in the latter part of the Cenozoic era. This is due to the continuous increase in $^{87}Sr/^{86}Sr$ ratios, which transition from approximately 0.7077 during the Bartonian period (around 40 million years ago) to 0.7092 in the Holocene epoch (McArthur et al., 2001). Strontium isotope chemostratigraphy remains viable across various periods of the Phanerozoic era, contingent upon the configuration of the Sr isotope profile. The significant synchrony observed between strontium isotope excursions and major Oceanic Anoxic Events (OAEs) during the Jurassic and Cretaceous periods suggests a plausible causal relationship (e.g., Jones and Jenkyns, 2001).

Considerable caution is necessary during the execution of strontium isotopic analyses to effectively correlate carbonate rocks of limestone and marl types, especially those younger than eight million years old (Howarth and McArthur, 1997). For the first time, Strontium isotope chemostratigraphy was applied to determine the depositional age of a previously unstudied sequence in terms of Sr isotope analyses, consisting of Serravallian-Aquitanian (Miocene) clayey limestones, limestones, and marls in the Kasaba Basin (Kaş-Antalya) region. Four carbonate samples were collected from the Kasaba Basin in the Kaş region (Antalya, Turkey), and $^{87}Sr/^{86}Sr$ analyses were conducted on these samples. One of these samples yielded a significantly high isotope value, although it did not provide a meaningful result, with the isotope ratio for this sample measured as 0.709459 ± 0.000026. However, three samples yielded results within a wide range, yet significantly meaningful, with measured ratios of 0.708267 ± 0.000025, 0.708790 ± 0.000026, and 0.708145 ± 0.000027, respectively (Fig. 21a, Table 2). The rocks in the study area have been dated paleontologically and isotopically for the

Epoch	Stage	Mediterranean Planktonic foraminiferal Zone Lirer et al. (2019)	Sample no	Planktonic foraminifera																				
				Globigerina bulloides	*Globigerinella obesa*	*Globigerinella siphonifera*	*Globigerinita uvula*	*Globigerinoides bollii*	*Globigerinoides extremus*	*Globigerinoides obliquus*	*Globoturborotalita apertura*	*Neogloboquadrina acostaensis*	*Neogloboquadrina atlantica*	*Globigerina bilobata*	*Orbulina suturalis*	*Orbulina universa*	*Sphaeroidinellopsis kochi*	*Sphaeroidinellopsis seminulina*	*Sphaeroidinellopsis sphaeroides*	*Trilobatus immaturus*	*Trilobatus quadrilobatus*	*Trilobatus sacculifer*	*Trilobatus trilobus*
MIOCENE	TORTONIAN	MMi 12a	GA 19						*						*	*								*
			GA 18												*	*								*
			GA 17						*						*	*								*
			GA 16													*		*			*			
			GA 15						*	*				*	*	*	*					*		*
			GA 14						*	*				*	*	*		*				*		*
			GA 13					*	*	*		*		*	*	*		*		*	*	*	*	*
			GA 12	*	*				*	*	*		*	*	*	*	*	*	*		*	*	*	*	*
			GA 11	*					*	*		*		*	*	*		*		*	*	*	*	*
			GA 10	*	*			*	*	*	*			*	*	*	*	*		*	*	*	*	*
			GA 9		*				*	*			*	*	*	*		*	*	*	*	*	*	*
			GA 8		*	*	*	*	*	*		*		*	*	*	*	*		*	*	*	*	*
			GA 7		*				*	*		*		*	*	*		*		*	*	*	*	*
			GA 6		*	*			*	*		*		*	*	*		*	*	*	*	*	*	*
			GA 5						*	*				*	*	*		*		*	*	*	*	*
			GA 4	*					*	*		*		*	*	*	*	*	*	*	*	*	*	*
			GA 3						*	*		*		*	*	*	*	*	*	*	*	*	*	*
			GA 2		*				*	*		*	*	*	*	*	*	*	*	*	*	*	*	*
			GA 1						*	*		*		*	*	*	*	*	*	*	*	*	*	*

Fig. 18. Distribution and biozone of planktonic foraminiferal assemblage of GA section.

first time. The stratigraphic trend of $^{87}Sr/^{86}Sr$ from the Pliocene to the Oligocene is illustrated in Fig. 21. The Miocene (Serravallian-Aquitanian) sequences in the Kasaba Basin have been estimated to range from 14.3 to 23.7 million years ago based on their strontium isotopic compositions (see Table 2; Fig. 21a).

Strontium isotope analyses were conducted on two samples from the Aksu-Gebiz Basin, similar to those collected from the Kaş-Kasaba Basin. The samples yielded $^{87}Sr/^{86}Sr$ ratios of 0.708924 and 1.709158, respectively. These results were evaluated in the relevant diagram (Fig. 21b–Table 1), and according to this analysis, the first sample indicates an age of 9.0 Ma, corresponding to the Tortonian, while the second sample suggests an age of 5.3 Ma, corresponding to the Messinian.

Age	Low Latitudes Zones Bolli and Sounders (1985)	Zones Blow (1969)	(Sub)Tropical Zones Berggren et al. (1995)		Tropical-Subtropical Zones Wade et al (2011)		Mediterranean: Iaccarino and Salvatorini (1982) Iaccarino (1985)	Mediterranean: Iaccarino et al. (2007)	Mediterranean: Lirer et al. (2019)	Southern Anatolian: This study
late MIOCENE	*Globorotalia humerosa*	N17	*G.tumida plesiotumida*	M14	*Globorotalia lenguaensis-Globorotalia tumida*	M14	*Globigerinoides extremus*	Non Distinctive Zone	Non Distinctive Zone	Non Distinctive Zone	
							Globorotalia conomiozea	*G.conomiozea gr.* MMi13: *T.quinqueloba* (c); *G.nicolae* (b); *G.miotumida-G.nicolae* (a)	*G.conomiozea gr.* MMi13: *T.quinqueloba* (d); *G.nicolae-N.acos.* (c); *G.nicolae* (b); *G.miotumida-G.nicolae* (a)	
	Globorotalia acostaensis	N16	*G.acostaensis-G.merotumida*	M13 *N.acostaensis/ Glz. lenguaensis*	*Globigerinoides extremus/ Globorotalia plesiotumida-Globorotalia lenguaensis*	M13b	*Globorotalia plesiotumida/ Globorotalia lenguaensis*	*G.obliquus extremus* MMi12: *Globorotalia suterae* (b); *G.extremus- G.suterae* (a)	*G.obliquus extremus* MMi12: *Globorotalia suterae* (b); *G.extremus- G.suterae* (a)	*G.obliquus extremus* MMi12: ? ; *G.extremus- G.suterae* (a)
								G.obliquus extremus-G.bulloideus		
				M13a	*Neogloboquad.acostaensis-Globigerinoides extremus/ Globorotalia plesiotumida*	M13a	*Neogloboquad.acostaensis*	*Globorotalia acostaensis*	*N. acostaensis* (MMi11)	*N. acostaensis* (MMi11)	

Fig. 19. Correlation table of planktonic foraminiferal zones among different regions.

5. Discussion

This study presents a comprehensive integration of biostratigraphy and strontium isotope stratigraphy to refine the Neogene chronological framework of the Kasaba and Aksu-Gebiz Basins in the Eastern Mediterranean. Unlike previous studies that primarily relied on micropaleontological markers or traditional lithostratigraphic correlations (Poisson et al., 2003; Karabıyıkoğlu et al., 2005a), this research provides

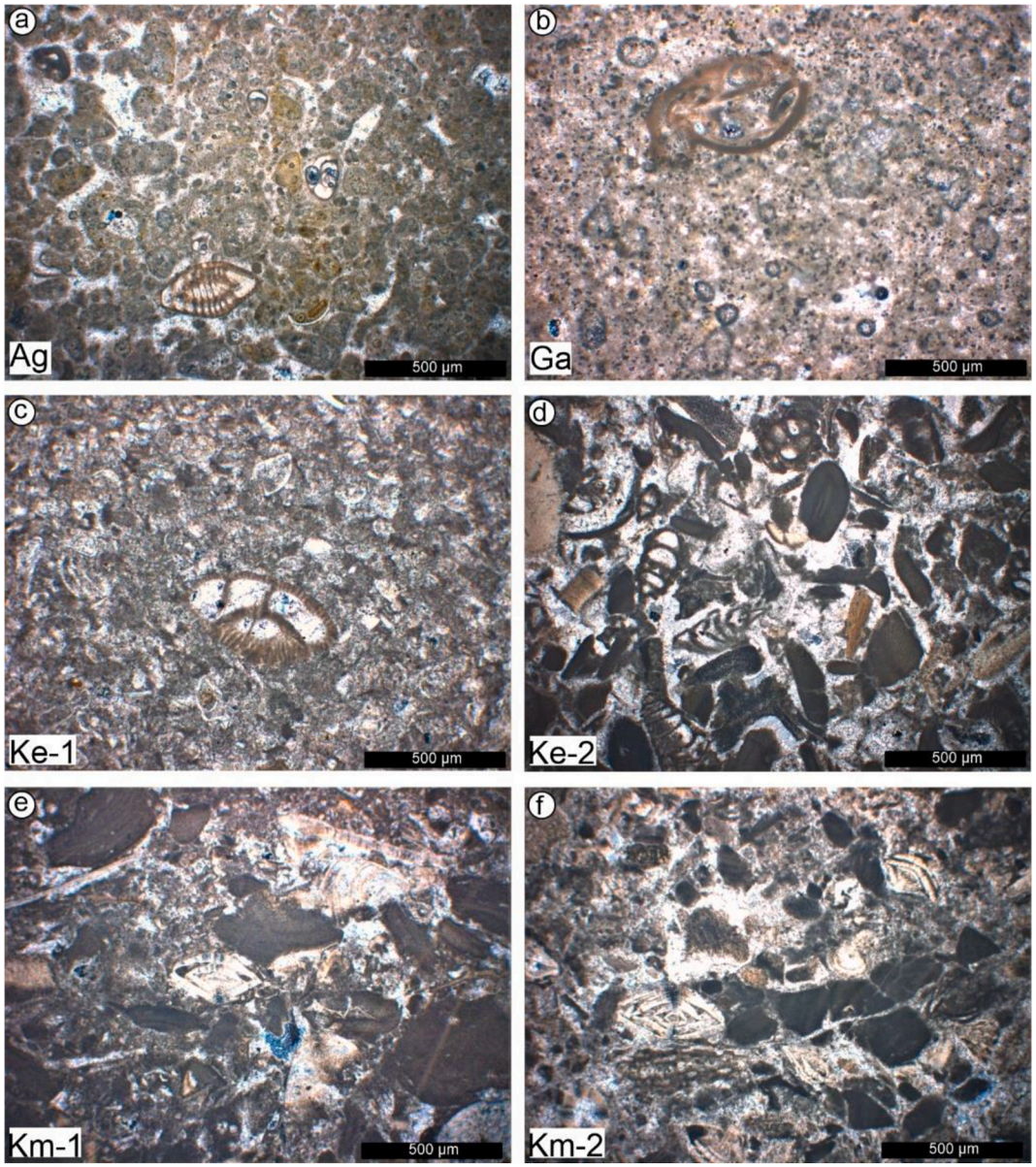


Fig. 20. Thin-section photomicrographs representing lithological characteristics of the Miocene transgressive carbonates and foraminiferal species within the study area of the Kasaba and Aksu basins; a) Intraclasts and microfossils observed within packstone, highlighting bioclast fragmentation and early diagenetic features, b) Grainstone, illustrating well-sorted grains and high intergranular porosity typical of high-energy depositional environments, c) Wackestone from the Ke-1 sample, characterized by a matrix-supported fabric with scattered bioclasts, d) A packstone sample of Ke-2 sample, displaying cementation with sparry calcite crystals filling the pore spaces, e) Microphotograph of a wackestone, showing a fine-grained micritic matrix and dispersed fossil fragments, f) Grainstone sample of Km-2 sample, illustrating tightly packed grains with evidence of grain-to-grain contacts and minimal matrix content.

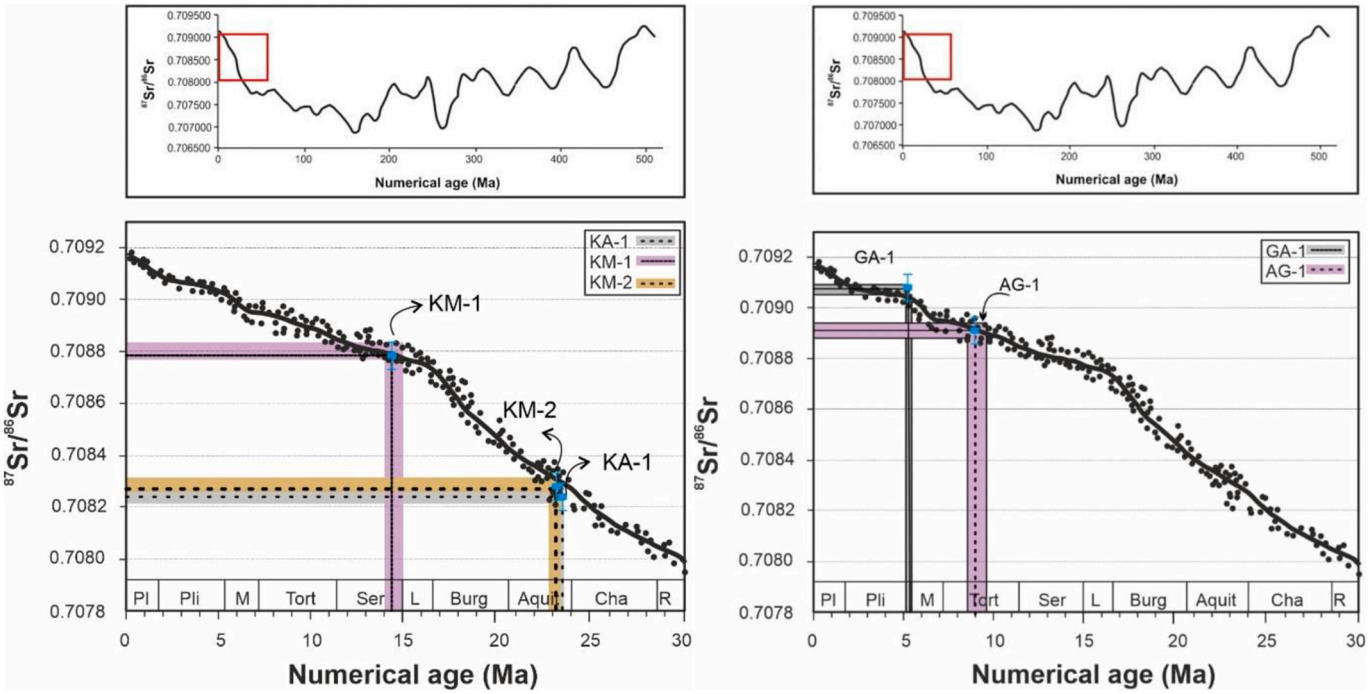


Fig. 21. a) The positions of three samples compiled from the Kasaba Basin (Kaş-Antalya) region on the $^{87}Sr/^{86}Sr$ isotope curve from the Pliocene-Oligocene period (The Strontium isotope variation curve spanning the Pliocene to Miocene interval (McArthur et al., 2001)), b) The positions of two samples compiled from the Aksu-Gebiz Basin (Antalya) region on the $^{87}Sr/^{86}Sr$ isotope curve from the Pliocene-Oligocene period. (The Strontium isotope variation curve spanning the Pliocene to Miocene interval (McArthur et al., 2001)).

Table 2
Strontium data and precise ages of the analyzed carbonate rocks.

Sample	$^{87}Sr/^{86}Sr$	2SE	Age (Ma)	Range (inc 2SE)	Stage
KM1	0.70879	26	14.2	14.0–14.9	Serravallian
KM2	0.708145	27	23.4	23.1–23.7	Aquitanian
KA1	0.708267	25	23.1	22.8–23.5	Aquitanian
KE1	0.709459	13	na	na	na
AG1	0.708924	30	9.0	8.6–9.7	Tortonian
GA1	0.709158	12	5.3	5.1–5.35	Messinian

a high-resolution temporal constraint through combined planktonic foraminiferal biostratigraphy and whole-rock Sr isotope analysis. The new data allow for a more precise understanding of basin evolution, particularly in relation to regional tectonic activity and its implications for flexural subsidence and sedimentary infill patterns. Studies on the Kasaba Formation, based on foraminiferal, paleogeographic, and chronostratigraphic data, show that it represents marine strata found in both the Mediterranean Tethys and the Central Paratethys during the lower and middle Miocene. Detailed biostratigraphic analysis of 30 samples from the Kasaba Formation reveals an abundance of planktonic foraminifera. In the KM section, 9 genera and 23 species were identified, while the KE section contained 12 genera and 29 species. These planktonic foraminifera were used to define the lower boundary of the Orbulina suturalis Lineage Subzone (MMi5a) of the *Orbulina suturalis-Globorotalia peripheroronda* Concurrent Range Zone (MMi5), which spans from the first appearance of *Orbulina suturalis* in the Langhian (middle Miocene) to the last occurrence of *Globorotalia peripheroronda*. This corresponds to the N9 Zone (Blow, 1969), the M6 Zone (Berggren et al., 1995), and the tropical-subtropical zonation (Wade et al., 2011). Only a few benthic foraminifera species were observed, mainly from shelf environments.

İslamoğlu (2004) determined the age of the Kasaba Formation as Langhian based on gastropod biostratigraphy, while İslamoğlu and Taner 2002a,b supported this with mollusk faunas. Sr isotopic data further support the Langhian age, with a boundary at the Serravallian-Langhian transition. The Kasaba Formation, characterized by shallow marine clastics, neritic limestone layers, and abundant marine fossils, reflects a shallow marine/coastal environment. Poisson (1977) suggested the formation's lower section is upper Burdigalian, with Langhian marls and conglomerates above, while Hayward (1982, 1984) proposed an upper Miocene fan delta environment. Other studies (Şenel et al., 1989; Tuzcu et al., 1994) also concluded the age range as upper Burdigalian to lower Langhian. The Kasaba Formation contains abundant benthic foraminifera, including *Ammonia* sp., *Cibicidioides* sp., and *Elphidium* sp., and exhibits a coarsening-upward trend from carbonate-rich deposits to siliciclastic units. These features indicate deposition in a shallow, warm marine environment with regressive characteristics, spanning the Langhian to Serravallian.

In the Aksu-Gebiz Basin, located approximately 100 km east and separated by the Lycian and Antalya Complex, the clastic Karpuzçay Formation and overlying carbonate-dominated Geceleme Formation represent two key Miocene marine units of the Eastern Mediterranean. Biostratigraphic analysis of 19 samples from the Karpuzçay Formation in the Gebiz (Aksu) region revealed abundant planktonic foraminifera in the first 12 samples, particularly *Lenticulina* sp., *Siphonina* sp., and *Bulimina* sp., which are indicative of a shelf environment. From the middle to upper sections, fossil content decreased (1–2 %), but benthic foraminifera, such as *Elphidium* sp., *Ammonia* sp., and *Nonion* sp., reflecting an inner shelf environment, were dominant. Planktonic species like *Orbulina universa*, *Globigerinoides extremus*, and *Trilobatus trilobus* were present throughout. The continuous presence of Globigerinoides extremus and the distribution of other planktonic foraminifera enabled the identification of the lower boundary of the MMi12a *Globigerinoides obliquus extremus-Globorotalia suterae* Interval Subzone, corresponding to the late Miocene (Tortonian), as defined by Lirer et al. (2019). This subzone aligns with Blow's (1969) N16 Zone, Berggren et al.'s (1995) M13b Subzone, and Wade et al.'s (2011) M13b Subzone in tropical-subtropical zonation.

İslamoğlu (2002) proposed an early Tortonian age for the Aksu

Formation in the Antalya Miocene Basin, refining the Tortonian age previously suggested by Akay et al. (1985b). In this study, the Karpuzçay Formation, which stratigraphically overlies the Aksu Formation, was assigned a general Tortonian age based on planktonic foraminifera fauna. Sr isotope data from the unit indicated a mid-Tortonian age. Karabıyıkoğlu et al. (2000), in their stratigraphic and sedimentological studies in the Manavgat Basin (southern Aksu Basin), also identified the Karpuzçay Formation as the final depositional stage during the Tortonian-Messinian period. Using the *Globorotalia acostaensis acostaensis* Biozone, they emphasized that, unlike the fault-controlled Çakallar member of the Geceleme Formation, the Karpuzçay Formation was influenced by a long-ranging tectonic phase associated with the northern shelf's uplift. Flecker et al. (1995) discussed similar tectonic and sedimentary processes in Miocene basins of southern Turkey, highlighting contrasting basin developments and their tectonic significance. Thus, the Tortonian age of the Karpuzçay Formation is confirmed, rather than a Serravallian age. In line with this, Karabıyıkoğlu et al. (2000) suggested that the Manavgat Basin could be compared to the westernmost part of the Adana Basin, located approximately 250–300 km to the east. Dündar and Varol (2014) studied the gypsum blocks within the Gebiz Formation (Manavgat Basin), overlying the predominantly clastic Karpuzçay Formation. These gypsum blocks, previously associated with Messinian reefal limestones, were extended to the early Pliocene, indicating a phase of uplift prior to reef deposition. These findings align with new Sr isotope results for the Gebiz Formation. Furthermore, the chaotic emplacement of gypsum over the Karpuzçay Formation suggests that the evaporite formation developed following a tectonic process that extended from the Tortonian to early Messinian.

Flecker et al. (1998) suggested that the sedimentation in the Aksu and Manavgat basins, located in front of the Lycian Nappes, was influenced by the increased flexural effects in the underlying lithosphere caused by the thrust load of the Lycian Nappes west of the Antalya Gulf. The asymmetric drainage system in these basins, which developed obliquely to the thrust front, can also be interpreted as a result of this process. However, in the northern parts of the Miocene Adana Basin, which has a similar lithological and stratigraphic basin system, different depositional episodes related to extensional regimes and normal faulting have been distinguished (Görür, 1992; Gürbüz, 1999; Ünlügenç and Akıncı, 2020). In this region, fan-delta deposition in the early Miocene was succeeded by reefal carbonate deposition in the middle Miocene, followed immediately by turbiditic deposition. The uplift at the end of the Miocene led to the formation of some debris-flow deposits that have now reached an elevation of 2000 m (Derman and Iztan, 1998).

The Kasaba and Aksu-Manavgat basins, which are adjacent and separated by tectonic slices like the Lycian Nappes, have undergone distinct tectono-sedimentary basin evolutions and are significant Miocene Eastern Mediterranean basins. In the west, ongoing nappe emplacement (Gülbahar Nappe) has influenced the units, while in the east, flexural tectonic effects in the Aksu-Manavgat basin have shaped the basin geometry and determined the depositional environment. Although the Miocene shelf environment in the west appears to have formed somewhat later than in the eastern basin, both basins exhibit discontinuities, short-term hiatuses, and facies changes associated with uplift and erosion events under the control of syn-sedimentary tectonic effects.

The findings from the Kasaba and Aksu-Gebiz Basins offer significant parallels and contrasts with other well-documented Neogene basins across the Mediterranean region. In the Western Mediterranean, the Betic-Rifian basins of southern Spain and Morocco exhibit similar transgressive-regressive cycles constrained by Sr isotope stratigraphy, yet their evolution was predominantly influenced by Atlantic-Mediterranean gateway dynamics rather than collision-related tectonics (Martín et al., 2009). The Apennine foreland basins in Italy also share depositional trends with the Kasaba Basin, particularly in terms of flexural subsidence driven by thrust emplacement; however, the new Sr isotope ages from this study provide a more refined depositional chronology compared to previous studies in the region (Mutti et al., 2003). In the Central Mediterranean, the Tunisian Neogene basins display broadly comparable biostratigraphic zonations, yet the recorded Sr isotope values exhibit minor deviations due to localized diagenetic overprints (Bouaziz et al., 2013). Similarly, the Ionian Basin in Greece underwent a comparable Late Miocene sedimentary evolution, yet its tectonic regime was primarily influenced by subduction-related extension rather than compressional flexural effects as observed in the Aksu-Gebiz Basin (Clews, 1989). In the Eastern Mediterranean, the Aksu-Gebiz Basin shares notable characteristics with the Cyprus basins, particularly in terms of Sr isotope fluctuations and Miocene transgressive sequences. However, while Cyprus records the final stages of Neotethyan subduction and related carbonate platform drowning (Robertson et al., 2024), the Aksu-Gebiz Basin reflects a more complex interplay between thrust-driven flexural subsidence and later extensional reactivation. Similarly, the Levant Basin (Israel, Lebanon) exhibits deep marine depositional settings throughout the Neogene, contrasting with the shallowing trends observed in the Kasaba and Aksu-Gebiz Basins due to regional uplift and increased siliciclastic input (Gvirtzman and Weissbrod, 1984).

Beyond the Mediterranean, Sr isotope stratigraphy has proven to be a powerful tool for refining depositional ages and correlating sedimentary successions in adjacent basinal settings. The Neogene sequence of the Dukhan Anticline (Qatar), as described by Dill et al. (2003), presents a similar approach in using sequence stratigraphy to delineate transgressive-regressive cycles. However, unlike the Kasaba and Aksu-Gebiz Basins, the Dukhan Anticline experienced relatively stable carbonate platform conditions with limited tectonic deformation. Further comparisons can be made with the Miocene Dam Formation in Qatar, where Dill and Henjes-Kunst (2007) applied Sr isotope and Ca isotope ratios to correlate stratigraphic sequences and infer paleoenvironmental conditions. While these studies highlight the effectiveness of Sr isotope geochemistry in constraining depositional histories, they lack the integration with micropaleontological data, which enhances the resolution of age models as demonstrated in this study. Moreover, Dill et al. (2009) examined diagenetic and epigenetic processes in organic-rich Cretaceous-Paleogene successions along the western margin of the Arabian Plate (northwestern Jordan). Their findings underline the influence of post-depositional geochemical alterations, a factor that has been carefully evaluated in the present study to ensure that Sr isotope values reflect primary seawater signals rather than diagenetic modification.

The Aksu-Gebiz Basin also shares similarities with the Hatay Graben (Southern Turkey), where a combination of Sr isotope geochronology and micropaleontology was used to refine the stratigraphy and tectonic history (Boulton et al., 2007). However, the Hatay Graben represents a predominantly extensional setting, whereas the Aksu-Gebiz Basin exhibits a more complex tectonic history, transitioning from thrust-induced subsidence to later extensional reactivation. In contrast to these previous studies, the integration of biostratigraphy and Sr isotope geochemistry in this research provides a more comprehensive and high-resolution approach to understanding basin evolution in the Eastern Mediterranean. The new data not only establish more precise depositional ages but also offer insights into the broader geodynamic framework, particularly the interaction between flexural subsidence, thrusting, and extensional reorganization.

The sedimentary evolution of the Aksu-Gebiz Basin during the Late Miocene was controlled by flexural subsidence followed by tectonic uplift, as evidenced by lithofacies transitions and changes in foraminiferal assemblages. The lower stratigraphic levels of the Karpuzçay Formation (Fig. 6) record an initial deep marine depositional environment, dominated by carbonate sedimentation and planktonic foraminiferal assemblages indicative of open marine conditions. As subsidence progressed, increased accommodation space facilitated the influx of siliciclastic material, reflected in the transition from carbonate-dominated facies to mixed carbonate-siliciclastic deposits. This phase

is marked by a shift in planktonic foraminifera, with decreasing abundance of oligotrophic species such as *Orbulina suturalis* and increasing representation of eutrophic taxa, suggesting enhanced terrestrial input. Further up in the sequence, a shallowing trend is observed, with the dominance of benthic foraminifera such as *Cibicidoides* and *Amphistegina*, which indicate inner shelf conditions. The uppermost stratigraphic levels reveal a transition from shallow marine carbonates to subaerial exposure, associated with a decline in planktonic foraminifera and an increase in marginal marine benthic taxa. This pattern aligns with tectonic reorganization, where flexural subsidence initially controlled sedimentation by creating accommodation space, while later uplift led to progressive shallowing and eventual regression of the basin.

This study's integration of biostratigraphy and Sr isotope stratigraphy refines the Neogene chronological framework for the Kasaba and Aksu-Gebiz Basins, significantly improving depositional age constraints, particularly for the middle-to-late Miocene transitions in the Aksu-Gebiz Basin. Unlike earlier studies that relied solely on micropaleontological markers (e.g., Poisson et al., 2003; Karabıyıkoğlu et al., 2005a), the combined approach here reduces age uncertainties and strengthens regional stratigraphic correlations. When compared to other Mediterranean Neogene basins, the Kasaba and Aksu-Gebiz Basins show similarities with the Betic-Rifian and Apennine foreland basins in depositional trends and Sr isotope variations (Martín et al., 2009; Mutti et al., 2003). However, the Kasaba Basin stands out due to more localized thrust-induced subsidence. Similarly, the Aksu-Gebiz Basin shares biostratigraphic zonations with the Ionian and Cyprus basins (Clews, 1989; Robertson et al., 2024), but its evolution was more strongly influenced by thrust-related flexural processes and later extensional reactivation. These results suggest that the Kasaba and Aksu-Gebiz Basins represent a transitional setting between large-scale Mediterranean foreland systems and localized collision-related basins in Anatolia.

6. Conclusions

The Kasaba and Aksu-Gebiz Basins record key stages in the Neogene sedimentary and tectonic evolution of the Eastern Mediterranean. The Kasaba Formation, based on biostratigraphic data, was deposited in a shallow, warm marine environment with regressive characteristics, spanning the Langhian to Serravallian. The presence of abundant benthic foraminifera such as *Ammonia* sp., *Cibicidioides* sp., and *Elphidium* sp. supports an inner shelf setting with increasing siliciclastic input over time. In the Aksu-Gebiz Basin, biostratigraphic data from the Karpuzçay Formation indicate a mid-Tortonian age, reflecting a transition from fine-grained siliciclastic deposition to carbonate platform development. The identification of planktonic foraminifera, including *Orbulina universa* and *Globigerinoides extremus*, further constrains the depositional age of these sequences. Strontium isotope analysis supports these biostratigraphic findings, with measured $^{87}Sr/^{86}Sr$ values yielding ages between 14.3 and 23.7 Ma for the Kasaba Basin and between 9.0 and 5.3 Ma for the Aksu-Gebiz Basin. The measured stratigraphic logs document a coarsening-upward trend in the Kasaba Basin, indicating a regressive depositional system, while the Aksu-Gebiz Basin exhibits a complex interplay of tectonic subsidence and carbonate accumulation. These findings highlight the role of tectonic activity in controlling sedimentation patterns and facies distribution in both basins. The integration of biostratigraphy, sedimentology, and Sr isotope stratigraphy refines the regional Neogene chronological framework and enhances correlations with adjacent basins. The results provide new insights into the tectono-sedimentary evolution of southwestern Anatolia, contributing to a broader understanding of the Neogene geological history of the Eastern Mediterranean.

CRediT authorship contribution statement

Ahmet Can Akıncı: Writing – review & editing, Writing – original draft, Visualization, Validation, Supervision, Software, Resources, Methodology, Investigation, Funding acquisition, Data curation, Conceptualization. **Nusret Nurlu:** Visualization, Methodology, Investigation, Conceptualization. **Ulvi Can Ünlügenç:** Supervision, Resources, Project administration, Funding acquisition. **Deniz İbilioğlu:** Writing – review & editing, Writing – original draft, Methodology, Data curation. **Hande Sonsun:** Writing – review & editing, Investigation.

Declaration of competing interest

The authors declare the following financial interests/personal relationships which may be considered as potential competing interests:

Ulvi Can UNLUGENC reports financial support was provided by Cukurova University. If there are other authors, they declare that they have no known competing financial interests or personal relationships that could have appeared to influence the work reported in this paper.

Acknowledgemets

We would like to thank to Department of Scientific Research Projects of Çukurova University (Adana/Turkey) for financial support to this study (Project No: FBA-2021-13454). We would also like to express our sincere gratitude to Dr. Serhat Köksal from METU for his invaluable assistance with the isotope analyses. We sincerely thank the reviewers and the editor for their constructive comments and suggestions, which have greatly improved the quality of our manuscript.

Data availability

Data will be made available on request.

References

Abdul Aziz, H., Di Stefano, A., Foresi, L.M., Hilgen, F.J., Iaccarino, S.M., Kuiper, K.F., Lirer, F., Salvatorini, G., Turco, E., 2008. Integrated stratigraphy and 40Ar/39Ar chronology of early middle Miocene sediments from DSDP leg 42A, site 372 (western mediterranean). Palaeogeogr. Palaeoclimatol. Palaeoecol. 257, 123–138.

Akay, E., Uysal, Ş., Poisson, A., Cravette, Y., ve Muller, C., 1985a. Antalya Neojen havzasının stratigrafisi. TJK Bul 28, 105–109.

Akay, E., Tüysüz, O., Işık, V., Sözbilir, H., 1985b. Geology of the Isparta Angle and adjacent areas. Geol. Soc. Am. Bull. 96, 10–29.

Akbaş, B., Akdeniz, N., Aksay, A., Altun, İ.E., Balcı, V., Bilginer, E., Bilgiç, T., Duru, M., Ercan, T., Gedik, İ., Günay, Y., Güven, İ.H., Hakyemez, H.Y., Konak, N., Papak, İ., Pehlivan, Ş., Sevin, M., Şenel, M., Tarhan, N., Turhan, N., Türkecan, A., Ulu, Ü., Uğuz, M.F., Yurtsever, A., et al., 2011. 1:1,250,000 Scale Geological Map of Turkey. General Directorate of Mineral Research and Exploration Publication, Ankara-Türkiye.

Akıncı, Ö., Robertson, A.H.F., Poisson, A., Bozkurt, E., 2003. Preface: the Isparta Angle, SW Turkey—its role in the evolution of tethys in the eastern mediterranean region. Geol. J. 38, 191–193. https://doi.org/10.1002/gj.952.

Aksarı, S., 2007. Gölova-Hacıyusuflar (Elmali, Antalya) Arasinin Jeolojisi. Selçuk Üniversitesi Fen bilimleri Enstitüsü. MsC Thesis, 104pp.

Aksoy, R., Aksarı, S., 2008. Elmali (Antalya, Batı Toroslar) Kuzeyinde Likya Naplarının jeolojisi. Selçuk Üniversitesi Mühendislik. Bilim Ve Teknoloji Dergisi 23 (2), 45–59.

Alçiçek, M.C., Kaymakcı, N., Yılmaz, Y., 2017. Discussion on "Neogene-Quaternary evolution of the Tefenni basin on the Fethiye-Burdur Fault Zone, SW Anatolia-Turkey". J. Afr. Earth Sci. 118, 137–148. https://doi.org/10.1016/j.jafrearsci.2016.12.009.

Alçiçek, H., Bülbül, A., Yavuzer, İ., Alçiçek, M.C., 2019. Hydrogeochemical and isotopic assessment and geothermometry applications in relation to the Karahayıt Geothermal field (Denizli basin, SW Anatolia, Turkey). Hydrogeol. J. 27, 1791–1816.

Barka, A., Reilinger, R., 1997. Active tectonics of the Eastern Mediterranean region: deduced from GPS, neotectonic and seismicity data. Ann. Geofisc. 40. https://doi.org/10.4401/ag-3892.

Ben-Avraham, Z., 1978. The structure and tectonic setting of the Levant continental margin, Eastern Mediterranean. Tectonophysics 46 (3–4), 313–331.

Berggren, W.A., Hilgen, F.J., Langereis, C.G., Kent, D.V., Obradovich, J.D., Raffi, I., et al., 1995. Late Neogene chronology: new perspectives in high-resolution stratigraphy. Geol. Soc. Am. Bull. 107 (11), 1272–1287.

Blow, W.H., 1969. Late middle Eocene to Recent planktonic foraminiferal biostratigraphy. In: Bronniman, P., Renz, H.H. (Eds.), Proc. First. Int. Conf. Planktonic Microfossils, Geneva, 1967, 1. E.J. Brill, Leiden, pp. 199–422.

Blumenthal, M.M., 1951. Isparta Angle: a significant morphotectonic structure in southwestern Anatolia. Bull. Miner. Res. Explor. Inst. Turk. 47, 1–15.

Bölükbaşı, A.S., Yoldemir, O., 1982. The geology of Beydağları between Kalkan-Elmalı-Kale (Demre) and petroleum possibilities. TPAO (Turkish Petroleum Corporation) Project No 1679, 1–117.
Bouaziz, S., Mouttaqi, A., Derrar, A., Jabour, H., 2013. Stratigraphic and structural framework of North African basins: petroleum systems and hydrocarbon potential. J. Afr. Earth Sci. 86, 1–21.
Boulton, S., Robertson, A.H.F., Ellam, R., Şafak, Ü., Ünlügenç, U.C., 2007. Strontium isotopic and micropalaeontological dating used to help redefine the stratigraphy of the neotectonic Hatay Graben, southern Turkey. Turk. J. Earth Sci. 16, 141–178.
Bozkurt, E., 2003. Origin of NE-trending basins in western Turkey. Geodin. Acta 16 (issues 2–6), 61–81.
Brandano, M., Policicchio, R., 2012. Strontium stratigraphy of the Burdigalian transgression in the western mediterranea. Lethaia 45, 315–328. https://doi.org/10.1111/j.1502-3931.2011.00285.
Burke, W.H., Denison, R.E., Hetherington, E.A., Koepnick, R.B., Nelson, H.F., Otto, J.B., 1982. Variation of seawater $^{87}Sr/^{86}Sr$ throughout Phanerozoic time. Geology 10, 516–519.
Cita, M.B., 1976. Planktonic foraminiferal biostratigraphy of the mediterranean Neogene. In: Takayanagi, Y., Saito, T. (Eds.), Progress in Micropaleontology, pp. 47–68.
Clews, J.E., 1989. Structural controls on basin evolution: Neogene to quaternary of the ionian zone, western Greece. J. Geol. Soc. 146 (3), 447–457. https://doi.org/10.1144/gsjgs.146.3.0447.
Colin, J.P., 1962. Geology of the Beydağları region. Rev. Geogr. Phys. Geol. Dyn. 4 (4), 309–325.
Collins, A.S., Robertson, A.H.F., 1998. Processes of late cretaceous to late Miocene episodic thrust-sheet translation in the lycian Taurides, SW Turkey. J. Geol. Soc. 155 (5), 759–772.
Çiner, A., Karabiyikoglu, M., Monod, O., Deynoux, M., Tuzcu, S., 2008. Late cenozoic sedimentary evolution of the Antalya basin, southern Turkey. Turk. J. Earth Sci. 17 (2008), 1–41.
Çiner, A., Doğan, B., Yıldırım, C., Akçar, N., Ivy-Ochs, S., Alfimov, V., Kubik, P.V., Schlüchter, C., 2015. Quaternary uplift rates of the Central Anatolian Plateau, Turkey: insights from cosmogenic isochron-burial nuclide dating of the Kızılırmak River terraces. Quat. Sci. Rev. 107, 81–97. https://doi.org/10.1016/j.quascirev.2014.10.007.
Darbaş, G., Gül, M., 2017. The stratigraphy of Dalaman-Ortaca-Göcek (Muğla-SW Turkey). Kahramanmaraş Sütçü İmam Üniversitesi Mühendislik Bilimleri Dergisi 20, 60–73. https://doi.org/10.17780/ksujes.304309.
De Paolo, D.J., Ingram, B.L., 1985. High-resolution stratigraphy with strontium isotopes. Science 227 (4689), 938–941.
Derman, A.S., Iztan, Y.H., 1998. Results of Geochemical Analysis of Seeps and Potential Source Rocks from Northern Turkey and the Turkish Black Sea. Memoirs-American Association of Petroleum Geologists, pp. 313–330.
Dewey, J.F., Hempton, M.R., Kidd, W.S.F., Şaroglu, F., Şengör, A.M.C., 1986. Shortening of continental lithosphere: the neotectonics of Eastern Anatolia — a young collision zone. In: Geological Society, vol. 19. Special Publications, London, pp. 1–36, 1.
Dill, H.G., Nasir, S., Al-Saad, H., 2003. Lithological and structural evolution of the northern sector of the Dukhan Anticline, Qatar, during the early Tertiary: with special reference to bounding surfaces of sequence stratigraphical relevance. GeoArabia (Manama) 8, 201–226.
Dill, H.G., Henjes-Kunst, F., 2007. Strontium ($^{87}Sr/^{86}Sr$) - and calcium ($^{44}Ca/^{40}Ca$ -$^{44}Ca/^{42}Ca$) isotope ratios of the Miocene Dam Formation in Qatar: Tools for stratigraphic correlation and environment analysis. GeoArabia (Manama) 12, 61–76.
Dill, H.G., Kus, J., Abed, A.M., Sachsenhofer, R.F., Abul Khair, H., 2009. Diagenetic and epigenetic alteration of Cretaceous to Paleogene organic-rich sedimentary successions typical of the western margin of the Arabian Plate, northwestern Jordan. GeoArabia (Manama) 14, 101–140.
D'onofrio, S., Giannelli, L., Iaccarino, S., Morlotti, E., Romeo, M., Salvatorini, G., Sampò, M., Sprovieri, R., 1975. Planktonic foraminifero of the Upper Miocene from some Italian sections and the problem of the lower boundary of the Messinian. Boll. Soc. Paleontol. Ital. 14, 177–196.
Dumont, J.F., Kerey, E., 1975. Basic geological study of southern lake of Eğirdir. Turk. Jeol. Kurumu Bul. 18, 169–174 (in Turkish with an abstract in English).
Dunham, R.J., 1962. Classification of carbonate rocks according to depositional texture. In: Ham, W.E. (Ed.), Classification of Carbonate Rocks, vol. 1. A.A.P.G. Memoir, pp. 62–84, 108-121.
Durutürk, B., 2018. Kaş-kalkan Arasinin Yapisal Unsurlari Ve Bu Sistem İçinde Gelişen Karbonat Damarlarinin Özellikleri (Antalya, Güneybati Türkiye). Hacettepe University, Ankara. MsC Tehesis. 83pp.
Dündar, S., Varol, B., 2014. Study of the gypsum blocks within the Gebiz Formation. J. Geol. 122 (4), 409–423.
Emiliani, C., 1955. Pleistocene temperatures. J. Geol. 63, 538–578.
Erakman, B., Meşhur, M., Gül, M.A., Alkan, H., Öztaş, Y., Akpınar, M., 1982. Fethiye-Köyceğiz-Tefenni-Elmalı-Kalkan arasında kalan alanın jeolojisi. Türkiye Altıncı Petrol Kongresi. Nisan, Ankara, sayfa, pp. 23–31.
Ersoy, Ş., 1990. The analysis of evolution and structurai items of the western Taurus - Lycia – nappes. Jeol. Muhendisligi Derg. 37, 5–16.
Faure, G., Mensing, T.M., 2005. Isotope Principle and Applications, third ed. John Wiley & Sons, Hoboken.
Faure, G., 1986. Principles of Isotope Geology. John Wiley & Sons, New York.
Flecker, R., Robertson, A.H.F., Poisson, A., Müller, C., 1995. Facies and tectonic significance of two contrasting Miocene basins in south coastal Turkey. Terra Nova 7 (2), 221–232.
Flecker, R., Kopf, A., Jurado-Rodríguez, M.J., 1998. Structural evidence for the nature of hiatal gaps in the Upper Cretaceous to Holocene succession recovered from the Eratosthenes Seamount. In: Proceedings-Ocean Drilling Program Scientific Results. National Science Foundation, pp. 517–526.
Folk, R.L., 1959. Practical petrographic classification of limestones. Bull. Am. Assoc. Pet. Geol. 43 (1), 1–38.
Fox, L.R., Wade, B.S., 2013. Systematic taxonomy of early-middle Miocene planktonic foraminifera from the equatorial Pacific ocean: integrated ocean drilling Proram, site U1338. J. Foraminifer. Res. 43 (4), 374–405.
Frijia, G., Parente, M., 2008. Strontium isotope stratigraphy in the upper Cenomanian shallow-water carbonates of the southern Apennines: short-term perturbations of marine Sr-87/Sr-86 during the oceanic anoxic event 2. Palaeogeogr. Palaeoclimatol. Palaeoecol. 261 (Issues 1–2), 15–29.
Garfunkel, Z., 1998. Constrains on the origin and history of the eastern Mediterranean basin. Tectonophysics 298, 5–35.
Glover, C.P., Robertson, A.H.F., 1998. Role of regional and local tectonics in the origin of the Late Cretaceous–Paleogene mélanges in the Mersin–Anamur area, southern Turkey. Tectonophysics 284 (3–4), 231–251.
Görür, N., 1992. A tectonically controlled alluvial fan which developed into a marine fan-delta at a complex triple junction: Miocene Gildirli Formation of the Adana Basin, Turkey. Sediment. Geol. 81 (3–4), 243–252.
Günay, Y., Bölükbaşı, S., Yoldemir, O., 1982. Beydağlarının stratigrafisi ve Yapısı. Türkiye petrol Jeologları Derneği. In: Türkiye Altıncı Petrol Kongresi, pp. 91–101.
Güneş, P., Aksu, A.E., Hall, J., 2018. Structural framework and deformation history of the western Cyprus Arc. Tectonophysics 744, 438–457. https://doi.org/10.1016/j.tecto.2018.07.023, 2018.
Gürbüz, K., 1999. Regional implications of structural and eustatic controls in the evolution of submarine fans: an example from the Miocene Adana Basin, southern Turkey. Geol. Mag. 136 (3), 311–319.
Gvirtzman, G., Weissbrod, T., 1984. The Hercynian geanticline belt of the Levant. Geol. Soc. Am. Bull. 95 (10), 1140–1150.
Hall, J., Aksu, A.E., King, H., Gogacz, A., Yaltırak, C., Çiftçi, G., 2014. Miocene–recent evolution of the western Antalya Basin and its linkage with the Isparta Angle, eastern mediterranean. Mar. Geol. 349, 1–23.
Hayward, A.B., 1982. Türkiye'nin güneybatısındaki Beydağları ve Susuzdağ masiflerinde Miyosen yaşlı kırıntılı tortulların stratigrafisi: TJK. Bull. (Arch. Am. Art) 25 (2), 81–89.
Hayward, A.B., 1984. In: Dixon, J.E., Robertson, A.H.F. (Eds.), Miocene Clastic Sedimentation Related to Emplacement of the Lycian Nappes and Antalya Complex, SW Turkey (In Geological Evolution of the Eastern Mediterranean Tethys, vol. 17. Spec. Publ. Geol. Soc. London, pp. 287–300.
Howarth, J.R., McArthur, J., 1997. Statistics for strontium isotope stratigraphy: a robust lowess fit to the marine Sr-isotope curve for 0 to 206 Ma, with look-up table for derivation of numeric age. J. Geol. 105, 441–456.
Iaccarino, S., Salvatorini, G., 1982. A framework of planktonic foraminifera biostratigraphy for early Miocene to Late Pliocene Mediterranean area. Paleontologia Stratigrafica ed Evoluzione 2, 115–125.
Iaccarino, S., 1985. Mediterranean Miocene and Pliocene planktic foraminifera. In: Bolli, H.M., Saunders, J.B., Perch-Nielsen, K. (Eds.), Plankton Stratigraphy. Cambridge Univ. Press, Cambridge, pp. 283–314.
Iaccarino, S.M., Premoli Silva, I., Biolzi, M., Foresi, L.M., Lirer, F., Turco, E., 2007. Practical Manual of Neogene Planktonic Foraminifera. International School on Planktonic Foraminifera, (Neogene Planktonic Foraminifera). Università di Perugia Press, pp. 1–180.
İslamoğlu, Y., Taner, A., 1999. Stratigraphy and tectonic evolution of the Miocene Kasaba Basin, southwestern Turkey. Turk. J. Earth Sci. 8 (3), 209–232.
İslamoğlu, Y., Taner, A., 2002a. Sedimentology and tectonic setting of the Burdigalian Sinekçi Formation, southwestern Turkey. Geol. J. 37 (4), 355–376.
İslamoğlu, Y., 2002. Biostratigraphy of the mollusk fauna in the Antalya Miocene Basin. Mar. Micropaleontol. 45 (1–2), 123–135.
İslamoğlu, Y., Taner, G., 2002b. Molluscan fauna and stratigraphy of the Uçarsu and Kasaba formations at Kasaba Miocene Basin (western Taurides, SW Turkey). Bull. Miner. Res. Explor. 125 (125), 31–57.
İslamoğlu, Y., 2004. Detailed gastropod biostratigraphy study in the Kasaba Miocene Basin. J. Foraminifer. Res. 34 (1), 1–15.
Jones, C.E., Jenkyns, H.C., 2001. Seawater strontium isotopes, oceanic anoxic events, and seafloor hydrothermal activity in the Jurassic and Cretaceous. Am. J. Sci. 301, 112–149.
Karabıyıkoğlu, M., Yaltırak, C., Özburan, M., Uzel, B., 2000. Stratigraphic and sedimentological studies in the Manavgat basin. Turk. J. Earth Sci. 9 (1), 45–56.
Karabıyıkoğlu, M., Tunoğlu, C., Demircan, H., 2005a. The oncolitic limestone and its paleontological significance in the Miocene of the Aksu Basin, southwestern Turkey. Geobios 38 (4), 473–489.
Karabıyıkoğlu, M., Tuzcu, S., Çiner, A., Deynoux, M., Örçen, S., Hakyemez, A., 2005b. Facies and environmental setting of the Miocene coral reefs in the Late-Orogenic fill of the Antalya Basin, western Taurides, Turkey: implications for tectonic control and sea level changes. Sedim Geol 173, 345–371.
Kaymakcı, N., Özdemir, A., Topuz, G., 2017. Fethiye-Burdur Fault Zone (SW Turkey): a myth? Geophys. Res. Abstr. 19, EGU2017–5443.
Kaymakcı, N., Langereis, C., Özkaptan, M., Özacar, A.A., Gülyüz, E., Uzel, B., Sözbilir, H., 2018. Paleomagnetic evidence for upper plate response to a STEP fault, SW Anatolia. Earth Planet Sci. Lett. 498, 101–115.
Kennett, J.P., Srinivasan, M.S., 1983. Neogene Planktonic Foraminifera: A Phylogenetic Atlas. Hutchinson Ross Publishing Co., Stroudsburg, p. 265.
Khain, V.E., 1984. Regional geodynamics. Alpine Mediter- Ranean Belt. Nedra Publishing, Moscow.

Koçyiğit, A., Özacar, A.A., 2003. Extensional neotectonic regime through the NE edge of the Outer Isparta Angle, SW Turkey: new field and seismic data. Turk. J. Earth Sci. 12 (1), 67–90.
Konak, N., Akdeniz, N., Çakır, M.H., 1990. Çal-Çivril-Karahallı Dolaylarının Jeolojisi, MTA Rapor No: 8945. Ankara.
Konak, N., 2002. 1/500.000 Türkiye Jeoloji Haritası İzmir Paftası,. In: Şenel, M. (Ed.), Maden Tetkik Ve Arama Genel Müdürlüğü.
Konak, N., Şenel, M., 2002. 1/500.000 Türkiye Jeoloji Haritası Denizli Paftası. In: Şenel, M. (Ed.), Maden Tetkik Ve Arama Genel Müdürlüğü.
Koşun, E., 2012. Facies characteristics and depositional environments of Quaternary tufa deposits, Antalya, SW Turkey. Carbonate Evaporite 27, 269–289.
Köksal, S., Toksoy–Köksal, F., Göncüoğlu, M.C., 2017. Petrogenesis and geodynamics of plagiogranites from Central Turkey (Ekecikdağ/Aksaray): new geochemical and isotopic data for genera-tion in an arc basin system within the northern branch of Neo-tethys. Int. J. Earth Sci. 106, 1181–1203.
Leckie, R.M., Bralower, T.J., Cashman, R., 2002. Oceanic anoxic events and plankton evolution: Biotic response to tectonic forcing during the mid-Cretaceous. Paleoceanography 17, 1041. https://doi.org/10.1029/2001PA000623.
Lirer, F., Foresi, L.M., Silvia Maria Iaccarino, S.M., Salvatorini, G., Turco, E., Claudia Cosentino, C., Sierro, F.J., Caruso, A., 2019. Mediterranean Neogene planktonic foraminifer biozonation and biochronology. Earth Sci. Rev. 196, 102869.
Loeblich, A.R., Tappan, H., 1988. Generic taxa erroneously regarded as foraminifers. In: Loeblich, A.R., Tappan, H. (Eds.), Foraminiferal Genera and Their Classification. Springer US, Boston, MA, pp. 726–730.
Macdougall, J.D., 1991. Radiogenic isotopes in seawater and sedimentary systems. In: Heaman, L., Ludden, J.N. (Eds.), Applications of Radiogenic Isotope Systems to Problems in Geology. NMCA Short Course Handbook. Mineralogical Association of Canada, Toronto, ON, pp. 337–364 (Chapter10).
Martín, J.M., Braga, J.C., Betzler, C., 2009. Controls on cenozoic carbonate platform development in the western Mediterranean. Sediment. Geol. 219 (1–2), 1–5.
McArthur, J.M., Kennedy, W.J., Chen, M., Thirlwall, M.F., Gale, A.S., 1994. Strontium isotope stratigraphy for the Late Cretaceous: direct numerical age calibration of the Sr-isotope curve for the U.S. Western Interior Seaway. Palaeogeogr. Palaeoclim. Palaeoecol. 108, 95–119.
McArthur, J.M., Howarth, R.J., Bailey, T.R., 2001. Strontium isotope stratigraphy: lowess version 3: best fit to the marine Sr-isotope curve for 0–509 Ma and accompanying look-up table for deriving numerical age. J. Geol. 109, 155–170.
McArthur, J.M., 2010. Strontium isotope stratigraphy. In: Ratcliffe, K.T., Zaitlin, B.A. (Eds.), Application of Modern Stratigraphic Techniques: Theory and Case Histories. SEPM Special Publication 94. SEPM (Society for Sedimentary Geology), Tulsa, OK, pp. 129–142.
McArthur, J.M., et al., 2012. Marine strontium isotope stratigraphy. Geol. Soc. Am. Bull. 124 (1–2), 34–53.
Monod, O., Kuzucuoğlu, C., Okay, A.İ., 2006. A Miocene Palaeovalley Network in the western Taurus (Turkey). Turk. J. Earth Sci. 15, 1–23.
Montañez, I.P., Osleger, D.A., Banner, J., Mack, L.E., Musgrove, M., 2000. Evolution of the Sr and C isotope composition of Cambrian oceans. GSA Today (Geol. Soc. Am.) 10, 1–7.
Mutti, M., Eberli, G.P., Betzler, C., 2003. Carbonate platform-slope systems: components and processes. In: Eberli, G.P., et al. (Eds.), Tectonic and Sedimentary Controls on the Evolution of the South Florida Carbonate Platform, vol. 75. SEPM Special Publication, pp. 141–168.
Nazik, A., 2004. Planktonic foraminiferal biostratigraphy of the Neogene sequence in the Adana Basin, Turkey, and its correlation with standard biozones. Geol. Mag. 141 (3), 379–387.
Önalan, M., 1979. Elmalı-Kaş (Antalya) arasındaki bölgenin jeolojisi. Doktora tezi, İstanbul Üniversitesi Fen Fakültesi Monografileri 29, 13.
Özgül, N., 2002. Türkiye'nin tektonostratigrafik birimleri. MTA Dergisi 124, 27–60.
Özsayın, E., Dirik, K., 2007. Quaternary activity of the Cihanbeyli and Yeniceoba Fault Zones: İnönü-Eskişehir fault system, Central Anatolia. Turkish J Earth Sci 16, 471–492.
Özsayın, E., Dirik, K., 2011. The role of oroclinal bending in the structural evolution of the Central Anatolian Plateau: evidence of a regional changeover from shortening to extension. Geol Carpath 62, 345–359.
Özsayın, E., Çiner, T.A., Rojay, F.B., Dirik, R.K., Melnick, D., Fernandez, D., Bertotti, G., Schildgen, T.F., Garcin, Y., Strecker, M.R., et al., 2013. Plio-quaternary extensional tectonics of the central Anatolian Plateau: a case study from the Tuz Gölü basin, Turkey. Turkish J Earth Sci 22, 691–714.
Palmer, M.R., Edmond, J.M., 1989. The strontium isotope budget of the modern ocean. Earth Planet Sci. Lett. 92 (1), 11–26.
Poisson, A., 1977. Recherces geologiques dans les Taurides occidentales (Turquie). Ph.D. Thesis, Université Paris-Sud Orsay.
Poisson, A., Wernli, R., Sağular, E.K., Temiz, H., 2003. New data concerning the age of the Aksu thrust in the south of theAksu valley, Isparta Angle (SW Turkey): consequences for the Antalya Basin and the eastern mediterranean. Geol. J. 38, 311–327.
Poisson, A., Orszag-Sperber, F., Koşun, E., Bassetti, M.A., Müller, C., Wernli, R., Rouchy, J.M., 2011. The late cenozoic evolution of the Aksu Basin (Isparta Angle; SW Turkey): new insights. Bulletin Société Géologique de France 182, 133–148.
Reilinger, R., et al., 2006. GPS constraints on continental deformation in the Africa-Arabia-Eurasia continental collision zone and implications for the dynamics of plate interactions. J. Geophys. Res. 111, B05411. https://doi.org/10.1029/2005JB004051.
Robertson, A.H.F., Dixon, J.E.D., 1984. Introduction: aspects of the geological evolution of the eastern mediterranean. In: Dixon, J.E.D., Robertson, A.H.F. (Eds.), The Geological Evolution of the Eastern Mediterranean, vol. 17. Geological Society, London, pp. 1–74.
Robertson, A.H., Kopf, A., 1998. Tectonic setting and processes of mud volcanism on the Mediterranean Ridge accretionary complex: evidence from Leg 160. Proc. Ocean Drill. Progr. Sci. Results 160. Chapter 50.
Robertson, A.H.F., 1998b. Tectonic significance of the Eratosthenes Seamount: a continental fragment in the process of collision with a subduction zone in the eastern Mediterranean (Ocean Drilling Program Leg 160). Tectonophysics 298 (1–3), 63–82.
Robertson, A.H.F., 1998a. Mesozoic-Tertiary tectonic evolution of the easternmost Mediterranean area: integration of marine and land evidence. Proc. Ocean Drill. Progr. Sci. Results 160. Chapter 54.
Robertson, A.H.F., 2000. Mesozoic-Tertiary tectonic-sedimentary evolution of a South Tethyan oceanic basin and its margins in southern Turkey. In: Bozkurt, E., Winchester, J.A., Piper, J.D.A. (Eds.), Tectonic and Magmatism in Turkey and the Surrounding Area, Geol., Soc., vol. 173. Spec., Pub., London, pp. 97–138.
Robertson, A.H.F., Parlak, O., Taslı, K., Solak, C., Dumitrica, P., Danelian, T., 2024. Lower Palaeozoic-Paleogene geological development of a deep-water rift (Güzelsu Corridor) along the northern continental margin of the southern Neotethys in the eastern mediterranean region: evidence from the Antalya complex and the adjacent tauride carbonate platform. Earth Sci. Rev. 252, 104741. https://doi.org/10.1016/j.earscirev.2024.104741.
Sarı, B., Özer, S., 2009. Upper cretaceous rudist biostratigraphy of the Bey Dağları carbonate platform, western Taurides, SW Turkey. Geobios 42 (3), 359–380. https://doi.org/10.1016/j.geobios.2008.10.006.
Schildgen, T.F., Cosentino, D., Bookhagen, B., Niedermann, S., Yıldırım, C., Echtler, H., et al., 2012. Multi-phased uplift of the southern margin of the Central Anatolian plateau, Turkey: a record of tectonic and upper mantle processes. Earth Planet Sci. Lett. 317, 85–95.
Shields, G.A., 2007. A normalised seawater strontium isotope curve: possible implications for Neoproterozoic-Cambrian weathering rates and the further oxygenation of the Earth. eEarth 2, 35–42.
Stampfli, G.M., Hochard, C., Vérard, C., Wilhem, C., 2013. The formation of Pangea. Tectonophysics 593, 1–19.
Şafak, Ü., Gökçen, N., 1991. Planktonik foraminifer zonlamasına doğu Akdeniz provensinden bir örnek: Mut havzası Tersiyer istifi. Turk. Jeol. Kurumu Bul. 34 (1), 27–37 (in Turkish).
Şafak, Ü., Subaşı, I.Y., 1998. Beşkonak-Altınkaya (Serik KD'su, Antalya) dolayı Miyosen istifinin mikropaleontolojik ve ortamsal özellikleri. Yerbilim. Derg. 11, 67–86 (in Turkish).
Şafak, Ü., Güney, A., Nurlu, N., Sonsun, H., 2023. Planktonic foraminiferal biostratigraphy, microfacies and mineralogy analyses of lower-middle Eocene and middle Miocene carbonates in the Silifke-Taşucu Region (Mersin, Southern Anatolia). J. Geol. Geophys. 12 (1), 10001062.
Şenel, M., Selçuk, H., Bilgin, Z.R., Şen, M.A., Karaman, T., Erkan, M., Kaymakçı, H., Örçen, S., Bilgi, C., 1987. Likya Napları ön cephe özellikleri (GB Türkiye). In: Türkiye Jeoloji Kurultayı Bildiri Özetleri, vol. 6.
Şenel, M., Selçuk, H., Bilgin, Z.K., Şen, M.A., Karaman, T., Dinçer, M.A., Durukan, E., Arbas, A., Örçen, S., ve Bilgi, C., 1989. Çameli (Denizli)- Yeşilova (Burdur)- Elmalı (Antalya) Ve Dolayının Jeolojisi. Maden Tetkik Ve Arama Rap. No: 9429 (Yayımlanmamış). Ankara.
Şenel, M., Bilgin, A.Z., Dalkılıç, H., Gedik, l., Serdaroğlu, M., Uğuz, F., Korucu, M., 1991. Eğirdir-Sütçüler- Yenişarbademli Arası Ve Yakın Dolayının (Batı Toroslar) Jeolojisi. Maden Tetkik Ve Arama Rap. No: 365 (yayımlanmamış), Ankara.
Şenel, M., Akdeniz, N., Öztürk, E.M., Özdemir, T., Kadınkız, G., Metin, Y., Öcal, H., Serdaroğlu, M., ve Örçen, S., 1994. Fethiye (Muğla)- Kalkan (Antalya) Ve Kuzeyinin Jeolojisi. Maden Tetkik Ve Arama Rap. No: 9761 (yayımlanmamış), Ankara.
Şenel, M., 1997. 1: 250 000 Ölçekli Türkiye Jeoloji Haritaları, Fethiye Paftası, No: 2, MTA, Jeo. Etüt. Dairesi, Ankara.
Şenel, M., et al., 1997. 1: 250 000 Ölçekli Türkiye Jeoloji Haritaları, Fethiye Paftası, No: 2, Maden Tetkik Ve Arama Genel Müdürlüğü. Jeoloji Etütleri Dairesi, Ankara.
Şenel, M., 2002. Türkiye Jeoloji Haritası. 1:500.000 Ölçekli Konya Paftası, vol. 14. Maden Tetkik ve Arama Genel Müdürlüğü, Ankara.
Şenel, M., 2004. Batı Toroslar'daki Yeşilbarak Napının stratigrafik ve yapısal özellikleri, GD Anadolu'daki ve Kuzey Kıbrıs'taki benzer birimlerle karşılaştırılması. MTA Dergisi 128, 1–26.
Taylor, A.S., Lasaga, A.C., 1999. The role of basalt weathering in the Sr isotope budget of the oceans. Chem. Geol. 161 (1–3), 199–214.
Toker, V., 1985. Korkuteli yöresi Miyosen nannoplankton biyostratigrafisi. Karadeniz Teknik Üniversitesi Dergisi. Jeoloji 4 (1–2), 9–21 (in Turkish).
Toker, V., Yıldız, A., 1991. Hatay yöresi nannoplankton biyostratigrafisi. In: Ahmet Acar Jeoloji Sempozyumu, pp. 199–211 (in Turkish).
Tunoğlu, C., Bilen, C., 2001. Burdigalian- Langhian (Miocene) ostracod biostratigraphy and chronostrattgraphy of the Kasaba basin (Kaş/Antalya). SW Turkey. Geol. Carpathica 52 (4), 247–258.
Tuzcu, S., Karabıyıkoğlu, M., İslamoğlu, Y., 1994. Batı Toroslar Miyosen Mercan resifleri: Bileşimleri, fasiyes özellikleri ve ortamsal konumları. 47. In: Türkiye Jeo. Kurultayı Bildiri Özetleri, vol. 16.
Ünlügenç, Ü.C., Akıncı, A.C., 2020. Sedimentary characteristics of early Miocene platform deposits in the Neogene AdanaBasin, southern Turkey. Turk. J. Earth Sci. 29 (4), 629–648.
Üner, S., Özsayin, E., Kutluay, A., Dirik, K., 2015. Polyphase tectonic evolution of the Aksu Basin, Isparta Angle (southern Turkey). Geol. Carpathica 66 (2), 157.
Üner, S., Özsayın, E., Dirik, R.K., Ciner, T.A., Karabıyıkoğlu, M., 2018. Reconstructing the sedimentary evolution of the Miocene Aksu Basin based on fan delta development (eastern Mediterranean-Turkey). Turk. J. Earth Sci. 27 (1), 32–48.

Veizer, J., Ala, D., Azmy, K., Bruckschen, P., Buhl, P., Bruhn, F., Carden, G.A.F., Diener, A., Ebneth, S., Godderis, Y., Jasper, T., Korte, C., Pawellek, F., Podlaha, O.G., Strauss, H., 1999. $^{87}Sr/^{86}Sr$, δ13C and δ18O evolution of Phanerozoic seawater. Chem. Geol. 161, 59–88.

Wade, B.S., Pearson, P.N., Berggren, W.A., Pälike, H., 2011. Review and revision of Cenozoic tropical planktonic foraminiferal biostratigraphy and calibration to the geomagnetic polarity and astronomical time scale. Earth Sci. Rev. 104 (1–3), 111–142.

Wasoo, M., Koç, A., 2021. Aksu Havzası'nın (Antalya, Türkiye) Neojen Stratigrafisi ve Yapısal Unsurları. Türkiye Jeoloji Bülteni 64, 83–128. https://doi.org/10.25288/tjb.682776.

Woodcock, N.H., Robertson, A.H.F., 1977. In: Imbricate Thrust Belt Tectonics and Sedimentation as a Guide to Emplacement of Part of the Antalya Complex SW Turkey (Second Edition, 1985). Abstracts, 6th. Colloquium Geology of the Aegean Region, İzmir-Turkey, pp. 661–671.

Yağmurlu, F., Bozcu, M., Şentürk, M., 2005. Burdur-Fethiye Arasındaki Bölgede Burdur Fayının Sismotektonik Özellikleri: Tübitak ÇAYDAG, Proje No:101Y027, 79 S. (Yayınlanmamış Rapor).

Yalçınkaya, S., Ergin, A., Afşar, Ö.P., Dalkılıç, H., Taner, K., Aksoy, Ö., Dağer, Z., Serdaroğlu, M., 1986. Batı Toroslar'ın Jeolojisi. MTA Derleme No:7898, Ankara (unpublished).

Yılmaz, Y.E., Atakul-özdemir, A., Koç, A., 2024. Manavgat havzasının (Antalya, Türkiye) Neojen Litostratigrafisi ve yapısal Unsurları. Turk. Jeol. Bul. 67 (1), 71–114. https://doi.org/10.25288/tjb.1291058.